DETECTION OF PIPELINE UPHEAVAL BUCKLING BY MEANS OF FIBRE-OPTIC SENSORS

A THESIS WRITTEN BY

ANDREA CARLINO

UNDER THE SUPERVISION OF

PROF. ALBERTO GODIO

FOR THE DEGREE OF

MASTER OF PETROLEUM ENGINEERING

MARCH 2020

INDEX

ACKNOWLEDGEMENTS

At the end of an arduous journey, travellers stop to recover strength and, before setting off again for new destinations, direct grateful thoughts to those who have guided, encouraged or merely accompanied them along the way. I am much obliged to my

- supervisor Prof. Godio, whose human qualities, passion and scientific competence have been profoundly inspiring;
- family (Father, Mother, Aunt Maria and the late Grandmother Antonia), which has taught me (in the words of Natalia Ginzburg) *not the little virtues but the great ones: not thrift but generosity and indifference to money, not prudence but bravery and contempt for danger, not astuteness but frankness and love of truth, not diplomacy but altruism and abnegation, not ambition but the desire to be and to know*. This will forever be my polestar.

PREFACE

One day a giant challenged Thor to raise his cat from the floor: the god of thunder grabbed it by the belly and began to lift; but the more he pulled, the more the feline arched its back. This mythological image (found in Snorri Sturluson's *Edda*) aptly summarises the salient features of upheaval buckling, a mechanism whereby a segment of buried pipeline (comparable to the extraordinarily stretchable creature of Norse fable) bows upwards out of the trench under excessive axial compression (analogous to the mighty effort expended by the hammer-wielding deity). Amongst the numerous factors determining the size of the involved force (e.g. mechanical properties of materials, impact of constraints, interaction with soil, loading history), elevated operating pressure (beyond 10 N/mm^2) and temperature (up to 100 °C above the external one) emerge as the most influential. The flowering of on- and (to a greater extent) offshore oil and gas fields worldwide has brought transport infrastructure into prominence: the possibility that overstress may culminate in rupture (with the attendant risks to man, nature and the economy) strongly calls for the adoption of continuous efficient reliable robust monitoring systems.

Today fibre-optic sensors offer an attractive alternative to their conventional electrical counterpart because they

- are light, versatile, cost-effective, safe to handle, of small diameter, resistant to corrosion and fatigue, immune to electromagnetic disturbance, unlikely to initiate fires or explosions, dielectric (ergo suitable for concrete and FRP);
- streamline the sensing architecture thanks to their dual role of gauges and pathways for signals;
- can be organised in serial and parallel multiplex arrays, which enable truly distributed measurements.

The present thesis aims at assessing the ability of such instruments to detect the upheaval buckling of pipelines. It is divided into three sections:

- the first examines the classical theory of buckling,
- the second discusses the key aspects of fibre-optic technology; starting from these conceptual premises,
- the third proceeds to analyse the results of a specially designed laboratory simulation.

A commitment is made to keeping the writing style concise and to the point, in pursuance of the maxim that *frustra fit per plura quod potest fieri per pauciora* ("it is vain to do with more what can be done with less"). Lastly, perusal of the appendices (amplifying the information imparted in the text) ought not to be omitted.

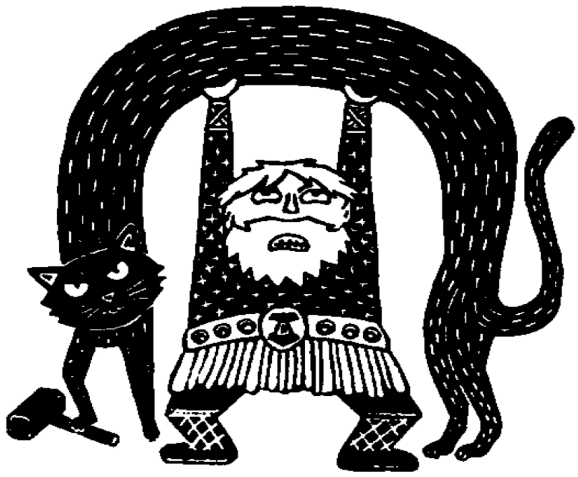

FIG. 1 Thor and the cat (linocut by Virginie Le Gall).

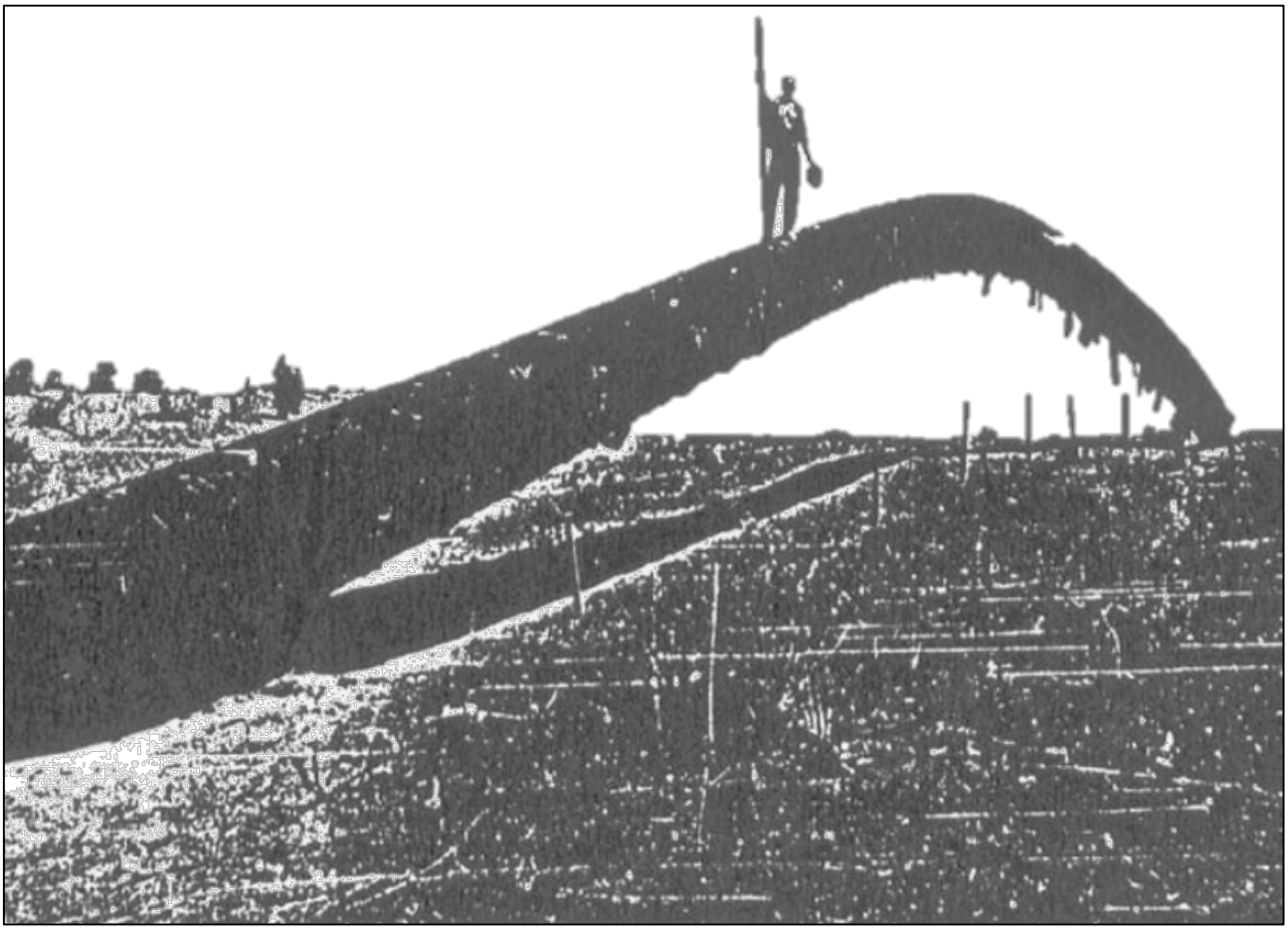

(a)

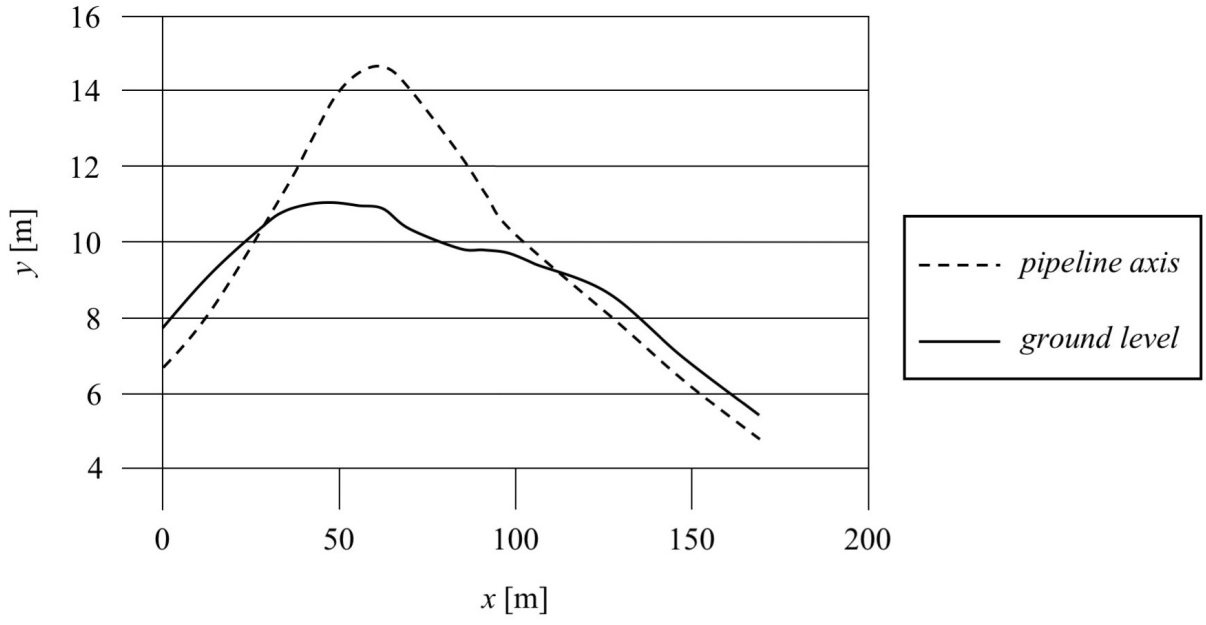

(b)

FIG. 2 (a) Photograph and (b) profile of a buckled 1020-mm (40-in.) onshore gas pipeline near Tashkent in Uzbekistan (adapted from Ref. 9, pp. 447-448).

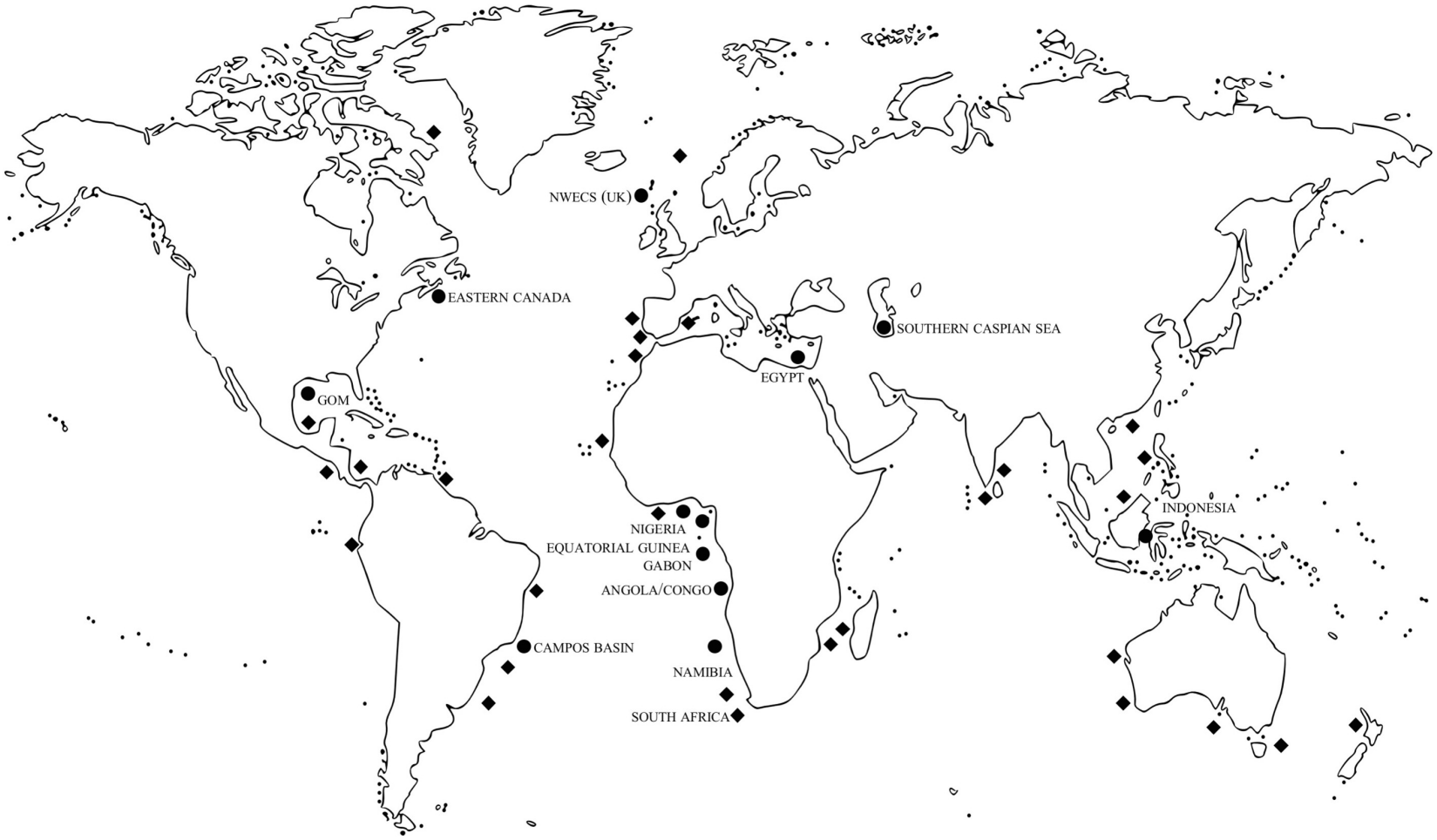

FIG. 3 Current (●) and future (♦) deep-water areas with proven hydrocarbon reserves (adapted from EDMUNDO CORONA, STELIOS KYRIAKIDES – *Buckling and collapse*, in *Mechanics of offshore pipelines*, Elsevier, 2007, vol. 1, p. 5).

TABLE 1

Examples of major on- and offshore pipelines (adapted from ibid., pp. 2-3)

	Trans-Alaska (USA)	*Trans-Mediterranean*	*Blue Stream*	*Medgaz*
Type	Onshore	On-/offshore	On-/offshore	On-/offshore
Product	Oil	Gas	Gas	Gas
From-to	Prudhoe Bay – Valdez	1. Hassi R'Mel (DZ) – Cape Bon (DZ) 2. Cape Bon – Mazara del Vallo (IT) 3. Mazara del Vallo – Mortelle (IT) 4. Mortelle – Favazzina (IT) 5. Favazzina – Bologna (IT)	1. Stavropol (RUS) – Dzhubga (RUS) 2. Dzhubga – Samsun (TR) 3. Samsun – Ankara (TR)	1. Hassi R'Mel (DZ) – Beni Saf (DZ) 2. Beni Saf – Almeria (E) 3. Almeria – Albacete (E)
Length [km]	1287	1. 920 2. 160 3. 352 4. 44 5. 1051	1. 370 2. 774 3. 501	1. 550 2. 200 3. 300
Capacity	800 Mstb/d	3 MMMscf/d	1.5 MMMscf/d	1.5 MMMscf/d
p *[bar]*	80	–	1. 75-100 2. 250 3. 75	–
Commissioned in	1977	1983	2003	2009
D ×t *[in.]*	48×0.462-0.562	1. 48 2. 20 3. 48 4. 10 + 20	1. 56 + 48 2. 24×1.254 3. 48×0.563	2. 24×1.170
Steel grade	X60, X65, X70	2. X65	2. X65	2. X70
Max. water depth [m]	n/a	2. 600 4. 360	2. 2150	2. 2160
Cost [$bn]	10	3	2.5	2. 0.75

TABLE 1 (CONT.)

	Baku-Ceyhan	*Mardi Gras (USA)*	*Independence Trail (USA)*	*Jansz & Gorgon Projects (AUS)*
Type	Onshore	On-/offshore	On-/offshore	On-/offshore
Product	Oil	Oil/gas	Gas	Gas
From-to	Baku (AZ) – Ceyhan (TR)	1. NaKika – MP 260 2. Thunder Horse – SP 89E 3. SP 89E – LOOP 4. Holstein/Mad Dog/Atlantis – Beaumont (via SS 332) 5. Holstein/Mad Dog/Atlantis – Neptune (via SS 332)	Independence Hub – Tennessee Gas Pipeline	1. Jansz Field – Barrow Island 2. Gorgon Field – Barrow Island
Length [km]	1760	1. 160 (Okeanos, gas) 2. 115 (Proteus, oil) 3. 145 (Endymion, oil) 4. 180 (Caesar, oil) 5. 180 (Cleopatra, gas)	220	1. 180 2. 70
Capacity	160 Mstb/d	1. 500 MMscf/d 2. 580 Mstb/d 3. 750 Mstb/d 4. 450 Mstb/d 5. 500 MMscf/d	850 MMscf/d	825 MMscf/d
p *[bar]*	–	–	–	–
Commissioned in	2006	2006	2007	2010
D ×t *[in.]*	42 + 36	1. 24 + 20×0.941-1.000 2. 28×1.088-1.210 + 24×1.095-1.200 3. 30 4. 28×1.045-1.148 + 20×0.971-1.227 5. 20×0.750-0.880 + 16×0.665-0.898	24	1. 24×1.236 + 28×1.173 2. 30×1.327
Steel grade	–	X65	–	X65
Max. water depth [m]	n/a	1310-2225	2450	1350
Cost [$bn]	3.6	1	0.28	–

1 UPHEAVAL BUCKLING OF PIPELINES

1.1 ANALYTICAL MODEL

The problem (according to Hobbs's formulation, reviewed by Calladine and Maltby) essentially concerns a long straight uniform heavy elastic pipe (assimilated to an Eulerian strut), laid on a flat rigid base at ambient temperature in stress-free conditions and constrained to lie in the vertical plane, regardless of the loads thereon exerted by its surroundings.

First, let T increase by a certain amount: the pipe would elongate with a strain

$$\varepsilon_1 = \alpha \Delta T \tag{1.1}$$

(α being the coefficient of linear thermal expansion) were it not assumed to be fastened to the base at either extremity; as a consequence, a compressive (positive) force is generated, equal to

$$P_1 = AE\alpha\Delta T, \tag{1.2}$$

in which A denotes the cross-sectional area and E the Young's modulus. By the same token, the axial strain due to the pressure p inside the pipe (characterised by an inner radius r, a wall thickness t and a Poisson's ratio ν)

$$\varepsilon_2 = \frac{1}{E}\left(\frac{pr}{2t} - \nu\frac{pr}{t}\right) \tag{1.3}$$

(here expressed in terms of the longitudinal and circumferential or hoop stresses in thin-walled cylindrical shells) is fully restrained, giving rise to

$$P_2 = \frac{Apr}{t}(0.5 - \nu). \tag{1.4}$$

In total,

$$P_0 = AE\alpha\Delta T + \frac{Apr}{t}(0.5 - \nu). \tag{1.5}$$

Next, following King and Palmer's approach, suppose that a single symmetrical buckle forms, having a height y, function of the horizontal distance x (it is convenient to locate the origin of the Cartesian coordinate system on the base, immediately below the apex); consider an infinitesimal element thereof, in translational and rotational equilibrium under the action of the normal force P, shear force S, bending moment M and weight per unit length w, wherefore

$$-S + wdx + (S + dS) = 0 \Rightarrow \tag{1.6}$$

$$\Rightarrow \frac{dS}{dx} + w = 0, \tag{1.7}$$

$$-M - wdx\frac{dx}{2} + P\frac{dy}{dx}dx - (S + dS)dx + (M + dM) = 0 \Rightarrow \tag{1.8}$$

$$\Rightarrow \frac{dM}{dx} + P\frac{dy}{dx} - S = 0. \tag{1.9}$$

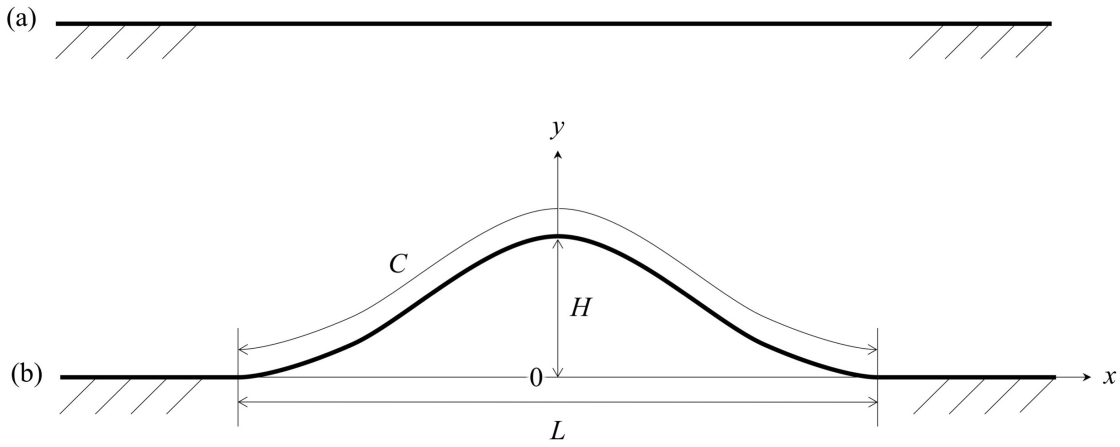

FIG. 1.1 (a) Straight pipe. (b) An upheaval buckle, with the coordinate system and principal dimensions. Note that the vertical scale is exaggerated.

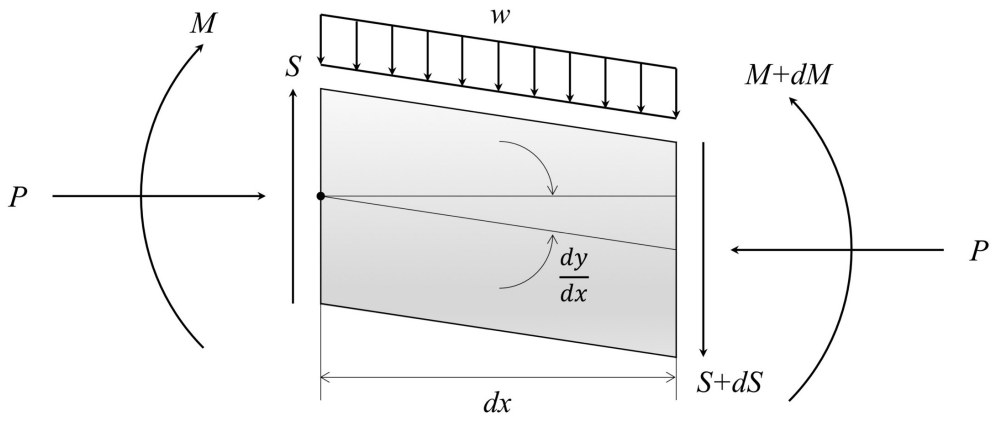

FIG. 1.2 Forces and moments acting on an element of the buckle.

Differentiation of (1.9) with respect to x and addition of (1.7) thereto lead to the governing equation

$$\frac{d^2M}{dx^2} + P\frac{d^2y}{dx^2} + w = 0. \tag{1.10}$$

Provided that $|dy/dx| \leq 0.1$ (hypothesis of small deflections and slopes), a proportionality subsists between M and curvature through flexural rigidity or stiffness (product of E and the second moment of area I):

$$M = EI\frac{d^2y}{dx^2}. \tag{1.11}$$

Finally, (1.10) can be rewritten as

$$EI\frac{d^4y}{dx^4} + P\frac{d^2y}{dx^2} + w = 0. \tag{1.12}$$

Now, naming the maximum height of the buckle H and the distance which separates the "peel" points L, the hereunder listed boundary conditions obtain:

$$y(0) = H, \tag{1.13}$$

$$y\left(\pm\frac{L}{2}\right) = 0, \tag{1.14}$$

$$\frac{dy}{dx}\left(\pm\frac{L}{2}\right) = 0, \tag{1.15}$$

$$\frac{d^2y}{dx^2}\left(\pm\frac{L}{2}\right) = 0. \tag{1.16}$$

(1.12-15) are fulfilled by

$$y(x) = \frac{wEI}{P^2}\left[1 + \frac{m^2L^2}{8} - \frac{m^2x^2}{2} - \frac{\cos(mx)}{\cos(mL/2)}\right] \tag{1.17}$$

(derived step by step in Appendix 1), which incorporates a wavenumber satisfying the relation

$$m^2 = \frac{P}{EI}; \tag{1.18}$$

whereas (1.16) requires that

$$\tan\frac{mL}{2} = \frac{mL}{2} \tag{1.19}$$

or, as lowest root,

$$mL = 8.99. \tag{1.20}$$

From (1.18) and (1.20),

$$P = 80.8\frac{EI}{L^2}. \tag{1.21}$$

Obviously, the contour of the pipe in the uplifted configuration C is greater than the original L, whence it ensues that P in the buckle must be less than P_0 away therefrom. This "geometric shortening" is computed from

$$C - L = \int_{-L/2}^{L/2} 0.5\left(\frac{dy}{dx}\right)^2 dx = \tag{1.22}$$

$$= 75.6\frac{w^2(EI)^{1.5}}{P^{3.5}}. \tag{1.23}$$

On the assumption (unrealistic in the case of actual pipelines, yet directly relevant to such short pin-ended tubes as those used in small-scale experiments) that slip along the base in the tracts flanking the buckle is completely prevented,

$$C - L = \frac{(P_0 - P)L}{AE}. \tag{1.24}$$

By equating (1.24) to (1.23),

$$P_0 = P + 16.0\times10^{-6}\frac{w^2AEL^6}{(EI)^2}, \tag{1.25}$$

with a minimum at

$$L_{min} = \left[1.69\times10^{6}\,\frac{(EI)^3}{w^2AE}\right]^{0.125}. \tag{1.26}$$

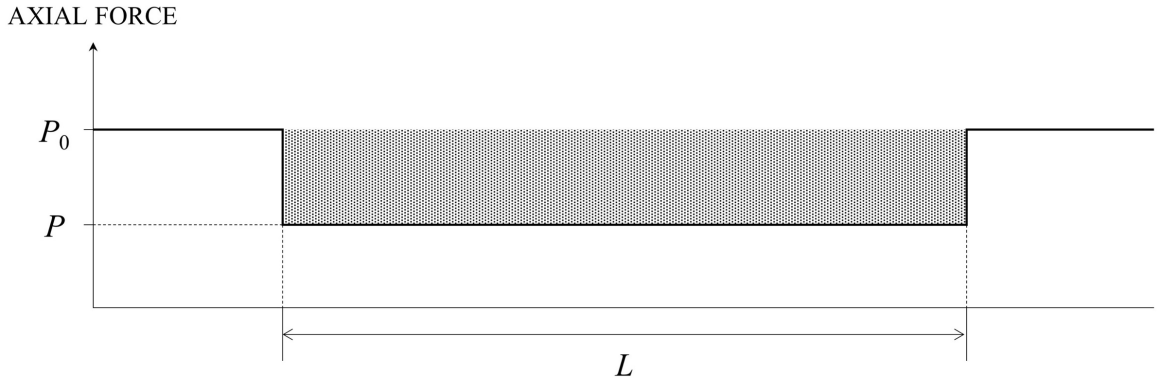

FIG. 1.3 Distribution of axial force in the buckled pipe. The stippled area is proportional to geometric shortening.

1.2 NUMERICAL EXAMPLE

Fig. 1.4 depicts (1.25) on a graph of P_0 against L, produced by a MATLAB script (v. Appendix 2) from data belonging to the experimental apparatus (v. Table 1.1). P_0 represents the control parameter of the phenomenon inasmuch as it is linked with ΔT and p by (1.5). Its curve falls sharply for small lengths (when the first summand on the right-hand side dominates) and, after crossing a minimum, climbs steeply as L grows (once the second takes over). Such a shape implies that

- a buckle cannot appear until $P_0 > P_{0,min}$;
- the equation admits two distinct solutions, associated to a shorter (always mechanically unstable) and a longer span respectively.

Plotting (1.21) makes it clear that $P_0 >> P$ for L big enough and their difference is proportional to geometric shortening in agreement with (1.24).

The transition from the unstable to the stable branch ("dynamic snap", $1 \rightarrow 2$) happens at lower forces and less dramatically in the presence of an initial crookedness, to be eventually replaced by a progressive enlargement of the imperfection (v. Fig. 1.5).

TABLE 1.1
Characteristics of LDPE PN-4 pipes (mfd. by Picenum Plast)

Parameter	*Symbol*	*Value*	*Unit*
Outer diameter	D	20*	mm
Wall thickness	t	1.6*	mm
Weight per unit length	w	0.000934*	N/mm
Yield strength	σ_y	14*	N/mm^2
Young's modulus	E	200*	N/mm^2
Thermal coefficient	α	200*	$\mu\varepsilon$/°C
Vicat softening temperature	VST	76-109**	°C
Poisson's ratio	ν	0.45***	–

* Italian Institute of Plastics.
** GEORGE WYPYCH – *Handbook of polymers*, ChemTech Publishing, 2016, p. 179.
*** ROY J. CRAWFORD – *Plastics engineering*, Butterworth-Heinemann, 1998, p. 59.

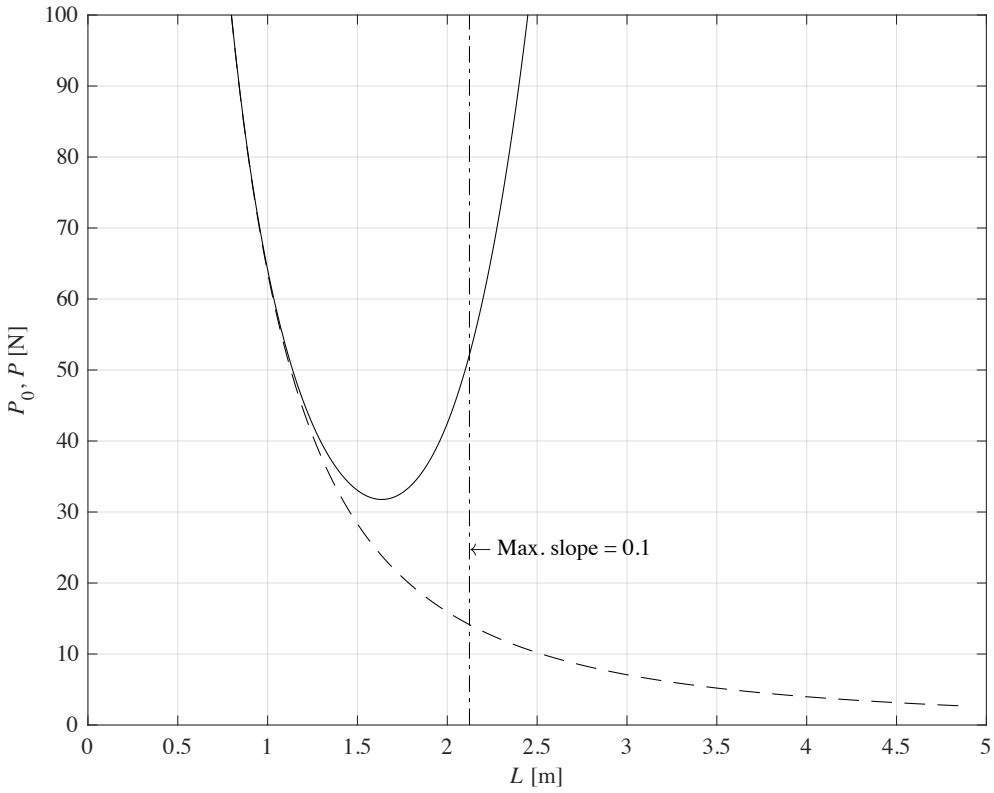

FIG. 1.4 P_0 (——) and P (– – –) vs L.

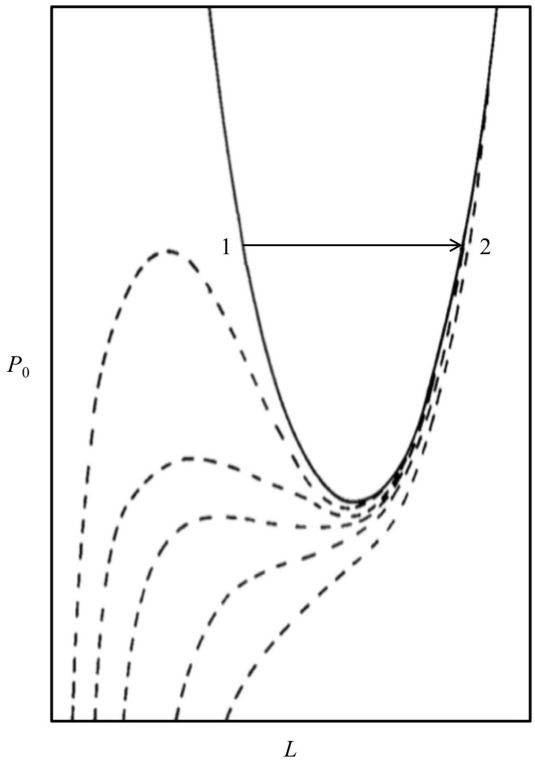

FIG. 1.5 Imperfection sensitivity of equilibrium paths (adapted from Ref. 8, p. 8).

2 FIBRE-OPTIC SENSING TECHNOLOGY

2.1 OPTICAL FIBRES

In his treatise (which constitutes the chief source of this section), Measures describes them as thread-like objects (approximately as fine as a strand of hair), drawn from highly pure fused silica (SiO_2) and capable of carrying light over vast distances with negligible loss. They consist of a core (within which rays propagate), surrounded and sustained by a cladding of lower refractive index n (minimising dissipation); moreover, an acrylate (or polyimide, when embedded in a composite material) coating safeguards against rapid disintegration by the agency of moisture. Employment in harsh environments may necessitate a tough protective jacket.

A common classification loosely distinguishes between single- and multimode fibres. In the former (whereon all interferometric sensors are based, including Bragg gratings – v. § 2.2), light travels as a plane wave (i.e. wavefronts are parallel planes perpendicular to the direction of propagation) inside a tiny core with a diameter of 5-10 μm, thus limiting the temporal spread of short pulses and widening the transmission bandwidth; whilst the latter can convey significantly greater power since they have a core diameter of up to 100 μm (ceteris paribus).

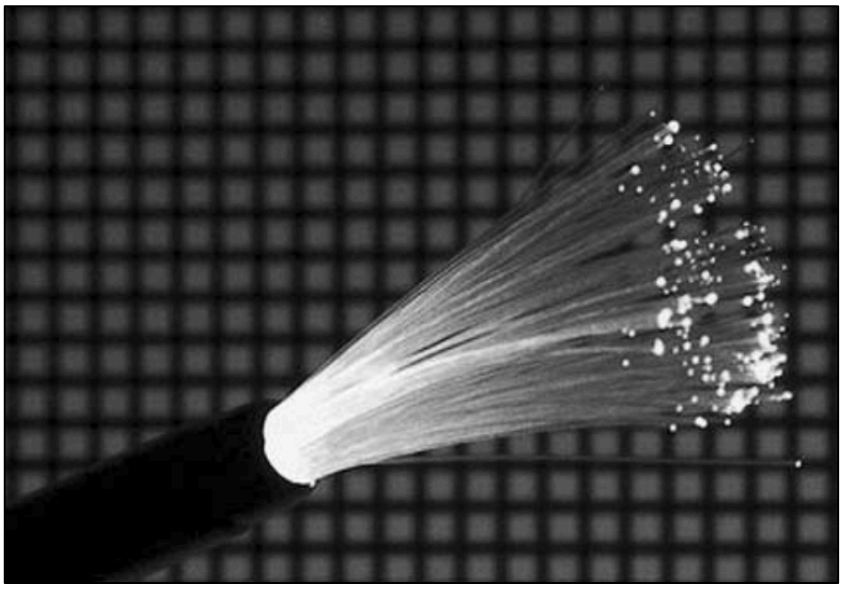

FIG. 2.1 Bundle of fibres (from Ref. 11, p. 161).

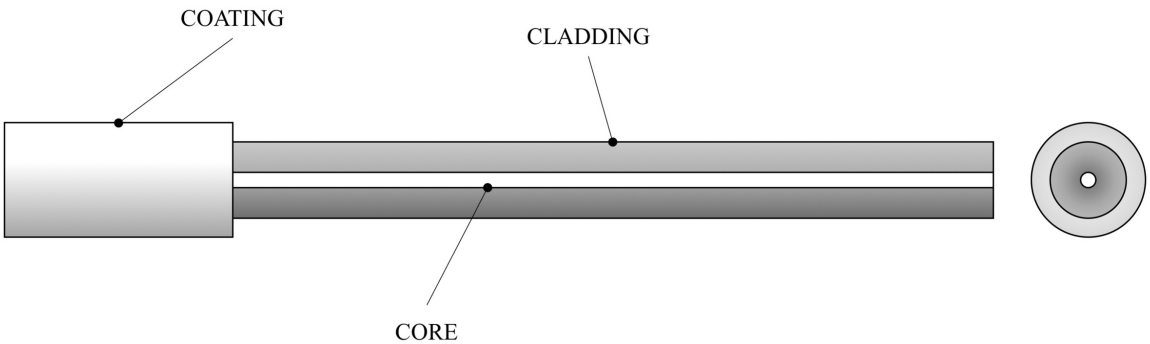

FIG. 2.2 Main parts of a fibre.

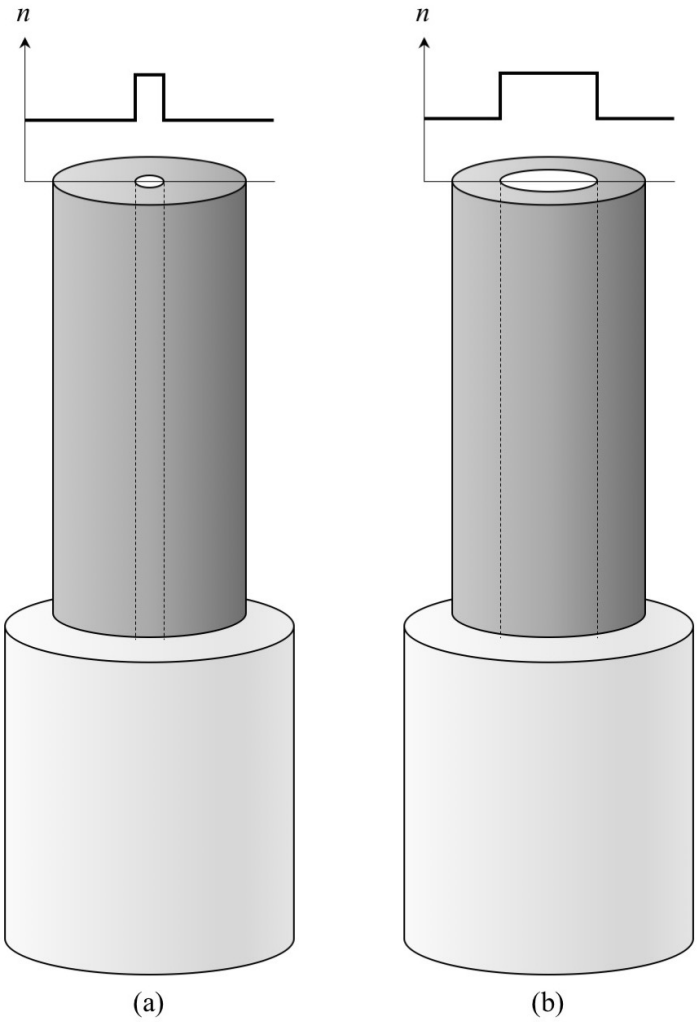

FIG. 2.3 Radial profiles of n for (a) single- and (b) multimode fibres.

2.2 FIBRE BRAGG GRATINGS

An FBG is a longitudinal sinusoidal variation in the n of a core, permanently induced by exposure to an intense interference pattern of ultraviolet light (an effect christened photosensitivity by its discoverer Hill in 1978). It serves as an excellent band-stop filter in that virtually no backscatter occurs from each consecutive peak in the aforesaid variation, save for wavelengths in the region of

$$\lambda_B = 2n\Lambda, \tag{2.1}$$

wherein Λ designates the grating period. Local changes in strain or temperature affect both parameters and hence linearly shift λ_B, thereby rendering the grating an intrinsic sensor (v. § 2.3).

The established procedure for fabricating FBGs entails photolithographically etching a 1D square-wave-profiled surface-relief structure on one of the faces of a silica-glass slab; such phase mask, being transparent to the incident UV radiation, diffracts it into the ±1 orders (the 0 one is supressed by properly adjusting the depth of corrugations), which interfere to create a periodic pattern, that imprints a grating (with $\Lambda = \Lambda_{mask}/2$, independent of the inscribing-beam λ) in the core.

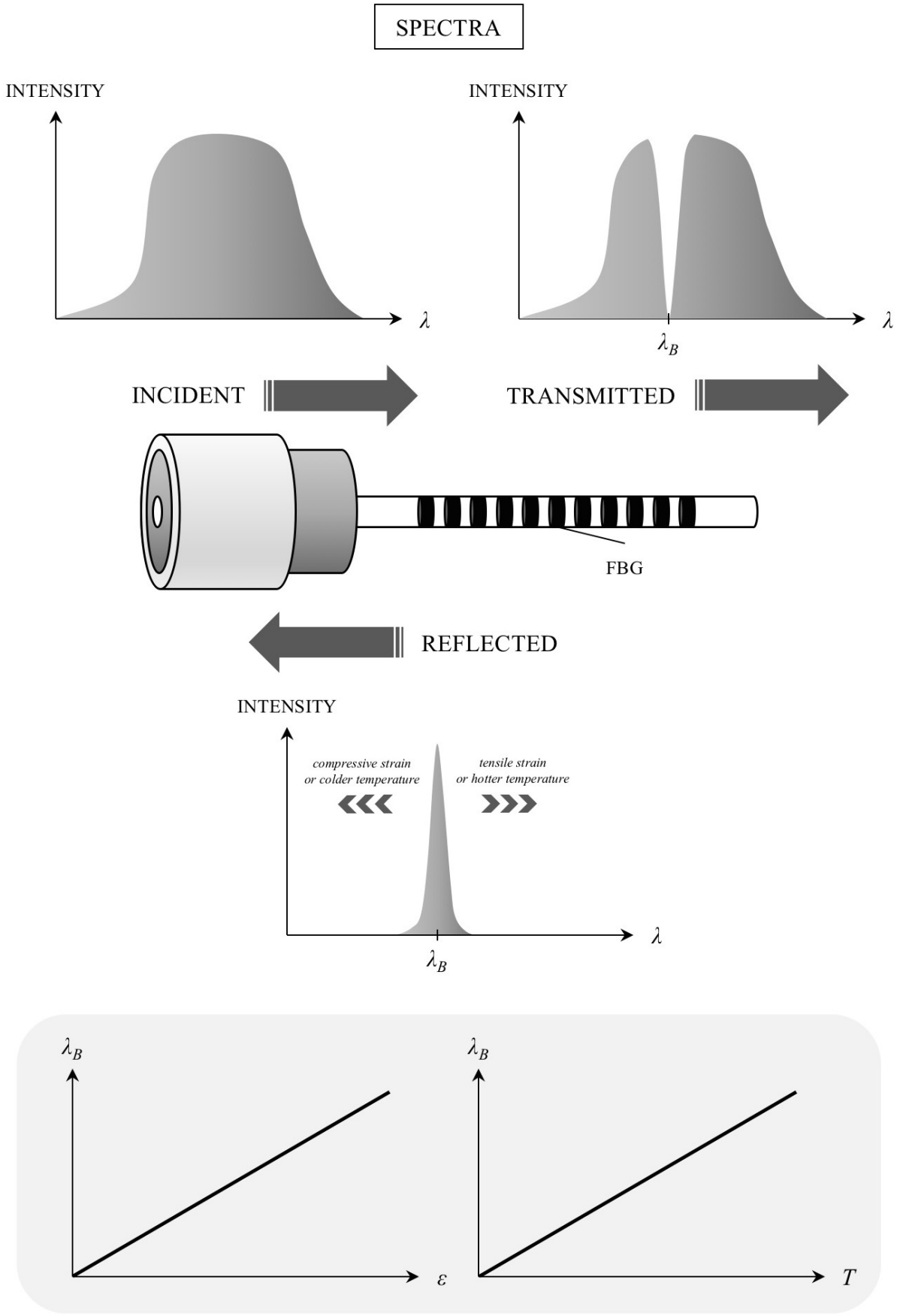

FIG. 2.4 Working principle of FBGs.

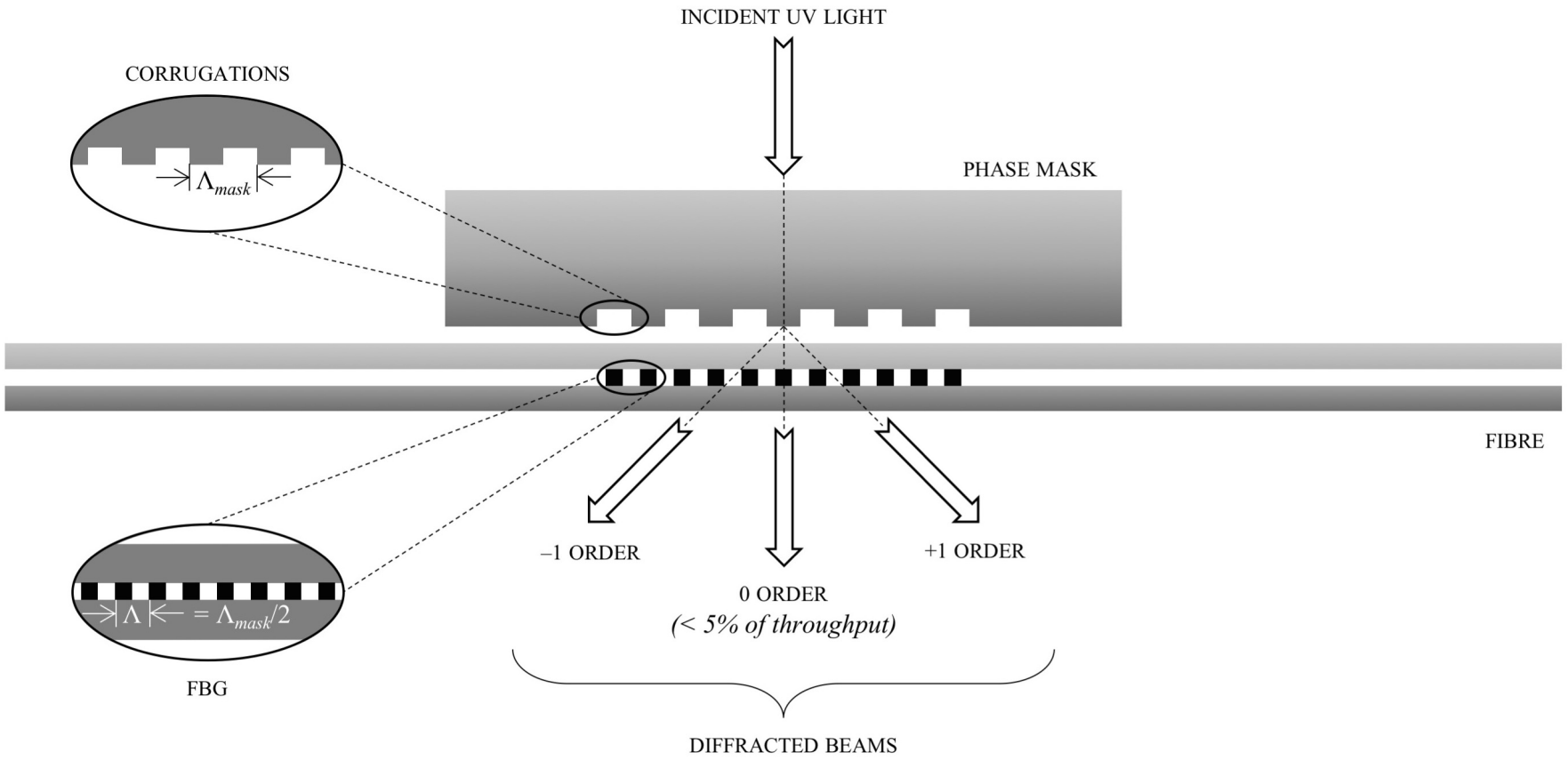

FIG. 2.5 Fabrication of FBGs.

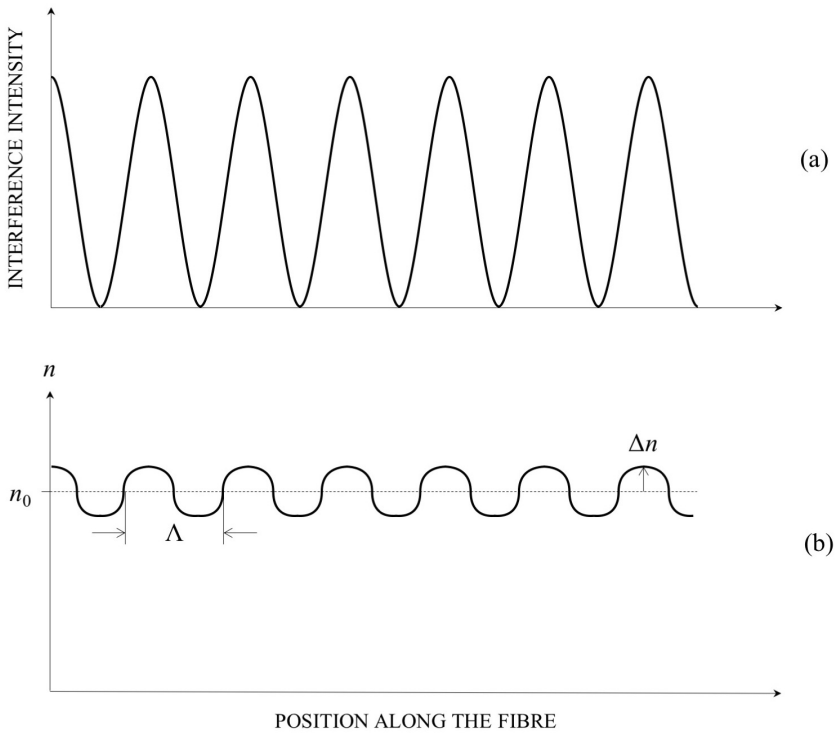

FIG. 2.6 (a) Interference pattern and (b) resultant variation in the *n* of a core.

2.3 OPTICAL-FIBRE STRAIN AND TEMPERATURE SENSITIVITY

The fundamental parameter of FBG sensors is the path length

$$\zeta_L = n\Lambda, \tag{2.2}$$

function of strain (or stress, in accordance with Hooke's law) and temperature as stated in § 2.2:

$$\zeta_L = \zeta_L(\sigma, T). \tag{2.3}$$

A 1st-order-truncated Taylor-series expansion of (2.3) gives

$$\Delta\zeta_L = \left(\frac{\partial\zeta_L}{\partial\sigma}\right)_T \Delta\sigma + \left(\frac{\partial\zeta_L}{\partial T}\right)_\sigma \Delta T; \tag{2.4}$$

here $(\partial\zeta_L/\partial\sigma)_T$ and $(\partial\zeta_L/\partial T)_\sigma$ symbolise the derivatives of ζ_L with respect to σ and T at a reference state (σ_0, T_0). In the light of (2.2), (2.4) can be further expanded as

$$\Delta\zeta_L = \left[n\left(\frac{\partial\Lambda}{\partial\sigma}\right)_T + \Lambda\left(\frac{\partial n}{\partial\sigma}\right)_T\right]\Delta\sigma + \left[n\left(\frac{\partial\Lambda}{\partial T}\right)_\sigma + \Lambda\left(\frac{\partial n}{\partial T}\right)_\sigma\right]\Delta T \Rightarrow \tag{2.5}$$

$$\Rightarrow \Delta\zeta_L = n\Lambda\left\{\left[\left(\frac{\partial\varepsilon}{\partial\sigma}\right)_T + \frac{1}{n}\left(\frac{\partial n}{\partial\varepsilon}\right)_T\left(\frac{\partial\varepsilon}{\partial\sigma}\right)_T\right]\Delta\sigma + \left[\left(\frac{\partial\varepsilon}{\partial T}\right)_\sigma + \frac{1}{n}\left(\frac{\partial n}{\partial T}\right)_\sigma\right]\Delta T\right\}. \tag{2.6}$$

If E and α of the fibre are introduced, (2.6) becomes

$$\Delta\zeta_L = n\Lambda\left\{\left[1 + \frac{1}{n}\left(\frac{\partial n}{\partial\varepsilon}\right)_T\right]\frac{\Delta\sigma}{E_F} + \left[\alpha_F + \frac{1}{n}\left(\frac{\partial n}{\partial T}\right)_\sigma\right]\Delta T\right\}, \tag{2.7}$$

the second addend in the first/second square bracket corresponding to the strain/thermo-optic effect. By defining the sensitivity to strain

$$S_\varepsilon \equiv 1 + \frac{1}{n}\left(\frac{\partial n}{\partial \varepsilon}\right)_T \tag{2.8}$$

and that to temperature

$$S_T \equiv \alpha_F + \frac{1}{n}\left(\frac{\partial n}{\partial T}\right)_\sigma, \tag{2.9}$$

(2.7) reduces to

$$\frac{\Delta\zeta_L}{\zeta_L} = S_\varepsilon \Delta\varepsilon + S_T \Delta T. \tag{2.10}$$

The normalised $\Delta\zeta_L$ and $\Delta\lambda_B$ are proportional, so that

$$\frac{\Delta\zeta_L}{\zeta_L} = \frac{\Delta\lambda_B}{\lambda_B}. \tag{2.11}$$

In conclusion, the basic structural-sensing equation (2.10) takes the form

$$\frac{\Delta\lambda_B}{\lambda_B} = S_\varepsilon \Delta\varepsilon + S_T \Delta T. \tag{2.12}$$

(2.12) suggests that any $\Delta\lambda_B$ caused by a deviation in temperature is indistinguishable from one ascribable to the application of an exclusively mechanical force; therefore, some sort of compensation is needed. Imagine that a fibre is installed on a host structure not subjected to external loads but experiencing only a ΔT; then an axial stress will develop therein, owing to the discrepancy in α:

$$\Delta\sigma = E_F(\alpha_H - \alpha_F)\Delta T. \tag{2.13}$$

Substitution of (2.13) into (2.12) yields

$$\frac{\Delta\lambda_B}{\lambda_B} = [S_\varepsilon(\alpha_H - \alpha_F) + S_T]\Delta T \tag{2.14}$$

and, allowing for stress-related strain,

$$\frac{\Delta\lambda_B}{\lambda_B} = S_\varepsilon[\Delta\varepsilon_m + (\alpha_H - \alpha_F)\Delta T] + S_T \Delta T. \tag{2.15}$$

Rearrangement of (2.15) delivers

$$\Delta\varepsilon_m = \frac{1}{S_\varepsilon}\frac{\Delta\lambda_B}{\lambda_B} - \Delta\varepsilon_T, \tag{2.16}$$

in which

$$\Delta\varepsilon_T \equiv \left(\alpha_H - \alpha_F + \frac{S_T}{S_\varepsilon}\right)\Delta T \tag{2.17}$$

stands for the apparent thermal strain. This can fatally vitiate measurements. By way of illustration, it was estimated that, given a $\Delta T = 96$ °C sufficient to trigger buckling in the Trans-Alaska Pipeline (v. Table 1), the $\Delta\varepsilon_T$ suffered by gauges of the kind under study herein (v. Fig. 2.7 and Table 2.1)

would far exceed $\Delta\varepsilon_m$: 1678 vs 393 $\mu\varepsilon$ (v. Appendix 3 for calculations). Even if α_H and α_F coincided, the fact that S_T is about an order of magnitude greater than S_ε could still pose serious difficulties.

Farrell et al. devised an interrogation technique which promises to overcome this drawback. In sketchy outline, the signal is sent from a broadband light source to an edge filter (FBG 1), split into a reference and a sensing arm (FBG 2), received by photodiodes (detectors). It is reiterated that a ΔT translates into a $\Delta\lambda_B$; by contrast, the shape (integral) of the reflected spectrum $G(\lambda)$ remains unaltered (v. Fig. 2.4). That being so, the ratio of the system

$$Q = 10\log_{10}\left[\frac{\int G_1(\lambda_{B1,0}+\Delta\lambda_{B1,T})G_2(\lambda_{B2,0}+\Delta\lambda_{B2,T}+\Delta\lambda_{B2,\varepsilon})d\lambda}{\int G_1(\lambda_{B1,0}+\Delta\lambda_{B1,T})d\lambda}\right] \tag{2.18}$$

simplifies to

$$Q = 10\log_{10}\left[\frac{\int G_1(\lambda_{B1,0})G_2(\lambda_{B2,0}+\Delta\lambda_{B2,\varepsilon})d\lambda}{\int G_1(\lambda_{B1,0})d\lambda}\right]. \tag{2.19}$$

None of the quantities in (2.19) pertains to T, so the technique is prima facie temperature-insensitive. Indeed, tests (v. Fig. 2.9) demonstrated that by increasing

- strain from 0 to 1100 $\mu\varepsilon$ at room temperature, Q decreases monotonically at a rate (slope) going successively up and down;
- T from 15 to 50 °C at a fixed strain of 320 $\mu\varepsilon$, $\Delta Q = \pm 0.15$ dB, meaning that $\Delta\varepsilon_T = \pm 2.2$ $\mu\varepsilon$ or $S_T = \pm 0.063$ $\mu\varepsilon$/°C (two orders of magnitude less than the value in Table 2.1).

For the sake of thoroughness, it is worth mentioning that, in similar fashion, the mismatch between the α's of the substrate and the measuring grid, combined with the dependence of the grid resistance on T, contributes to the "thermal output" exhibited by electrical sensors; however, as shown in Fig. 2.11, the temperature drift of a resistive gauge is substantially less severe than that of an optical one mounted on various supports.

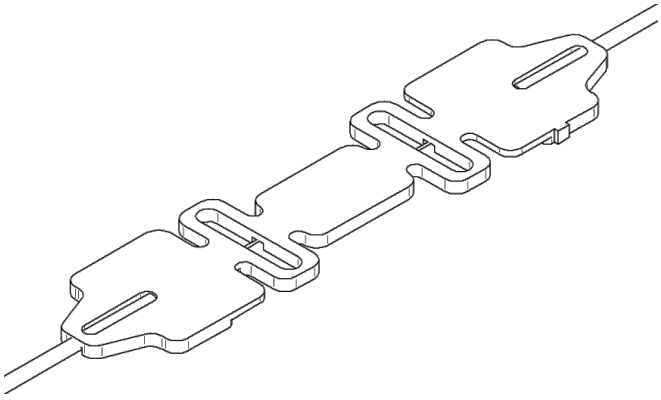

FIG. 2.7 FBG strain gauge (mfd. by Micron Optics) and...

TABLE 2.1
...its characteristics

Parameter	*Symbol*	*Value*	*Unit*
Bragg wavelength	λ_B	1532-1552*	nm
Strain sensitivity	S_ε	10^{-6}*	/$\mu\varepsilon$
Temperature sensitivity	S_T	6.156×10^{-6}*	/°C
Thermal coefficient	α_F	0.7	$\mu\varepsilon$/°C

* At 22 °C.

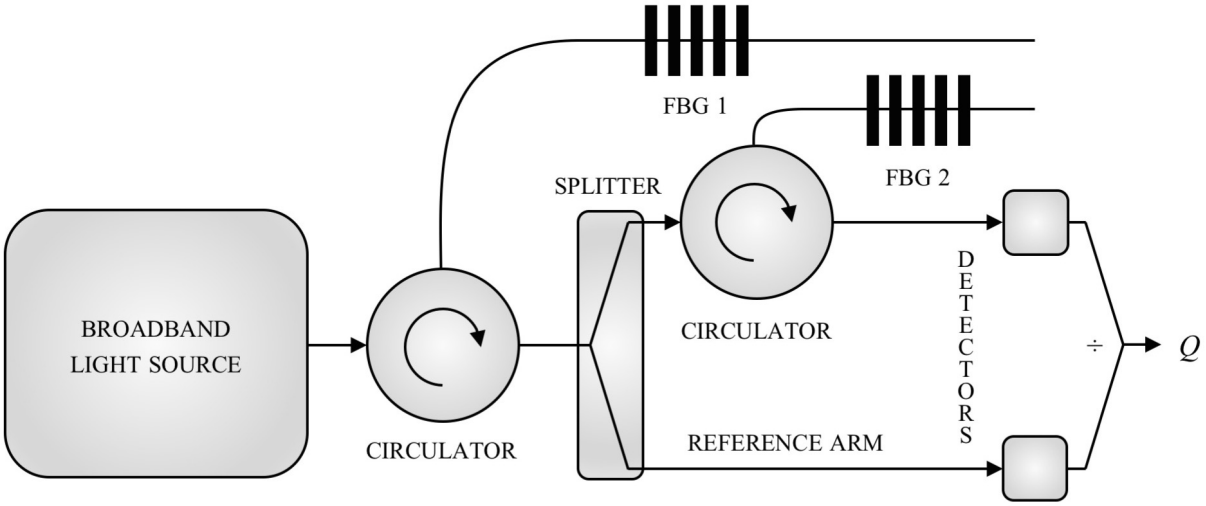

FIG. 2.8 Diagram of a temperature-insensitive interrogation technique for FBG sensors (adapted from Ref. 6, p. 654).

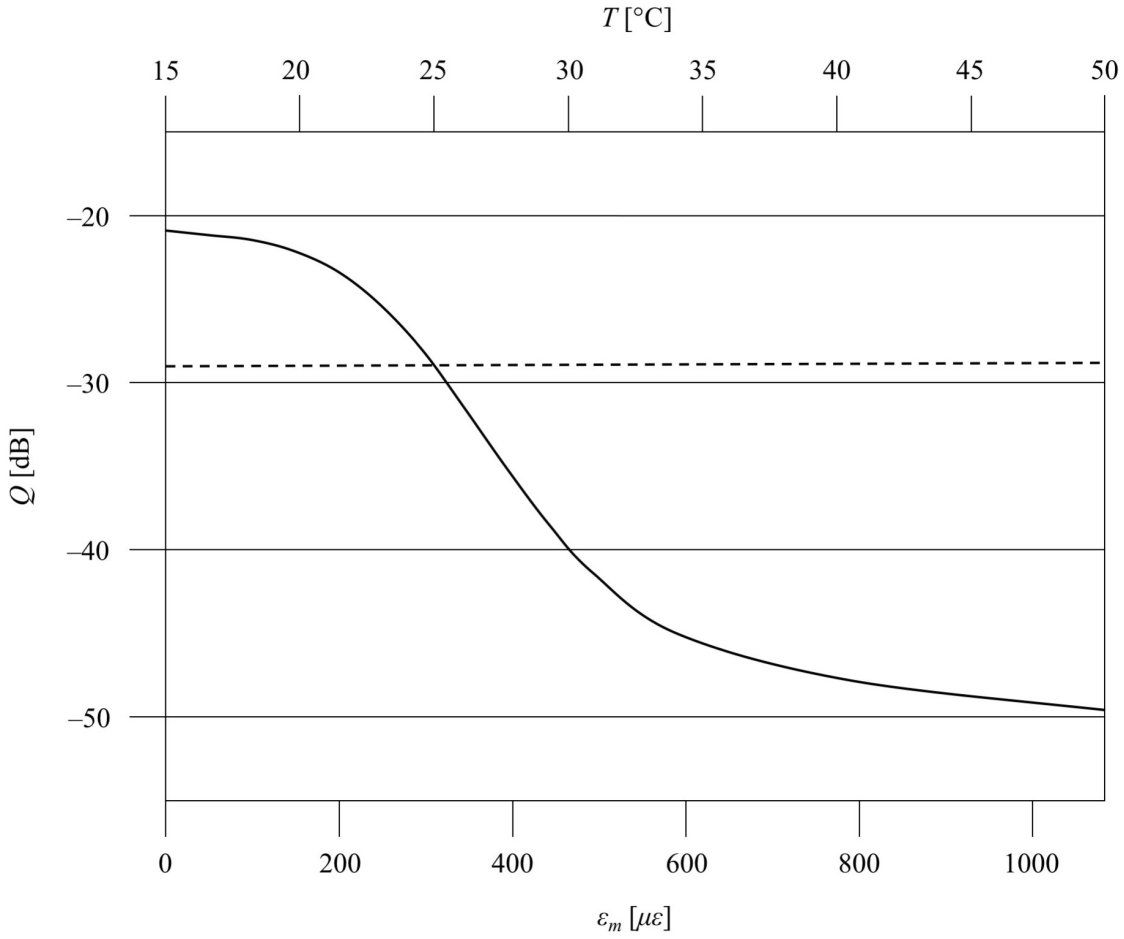

FIG. 2.9 Q vs ε_m at room temperature (——) and T at a fixed strain (– – –) (adapted from ibid., p. 655).

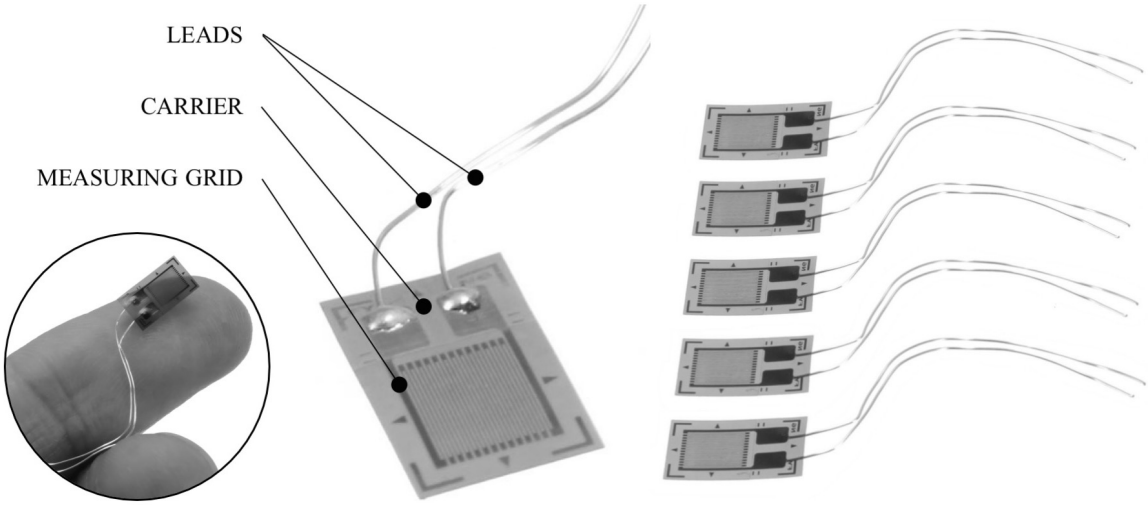

FIG. 2.10 Electrical strain gauges.

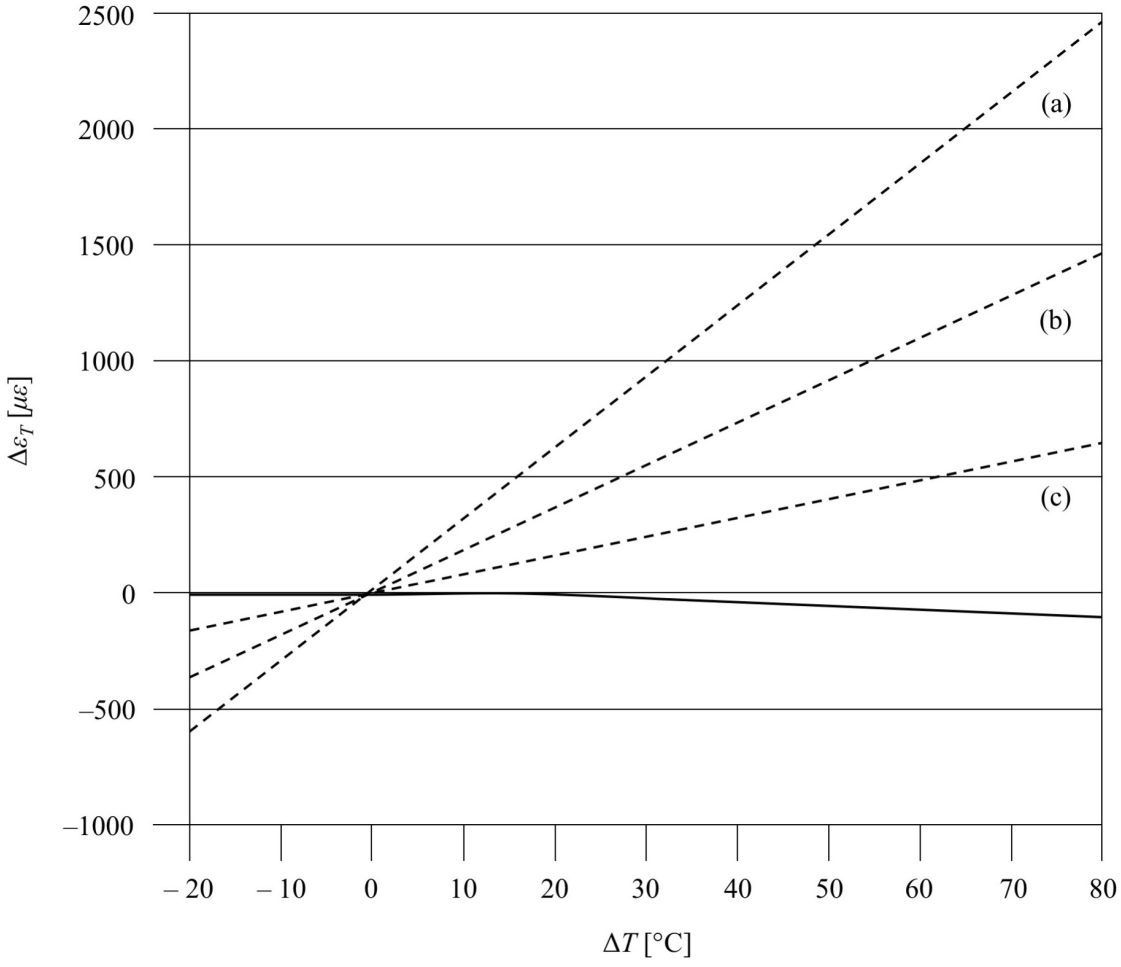

FIG. 2.11 $\Delta\varepsilon_T$ vs ΔT for an electrical (——) and an optical gauge (– – –) attached to (a) aluminium / (b) steel / (c) glass (adapted from Ref. 10, p. 227).

3 LABORATORY SIMULATION

3.1 MODUS OPERANDI

The longitudinal strain at an arbitrary point on the exterior of a buckled pipe of outer radius R, distant h from the neutral axis and making with it an angle θ comprises an axial and a bending component:

$$\varepsilon_l = \varepsilon_a + \varepsilon_b \tag{3.1}$$

or, equivalently,

$$\varepsilon_l = \varepsilon_a + \varepsilon_{b,max} \sin\theta, \tag{3.2}$$

wherein

$$\varepsilon_a = \frac{P_0 - P}{AE}, \tag{3.3}$$

$$\varepsilon_b = \frac{Mh}{EI}, \tag{3.4}$$

$$\varepsilon_{b,max} = \varepsilon_b|_{\theta=\pi/2} = \frac{MR}{EI}. \tag{3.5}$$

(3.2) is insoluble for it contains three unknowns (ε_a, $\varepsilon_{b,max}$, θ), unless as many measurements of ε_l per cross section are performed. Ansari et al. proposed that sensors should be placed at intervals of 120° around the circumference (that is to say, at 12, 4 and 8 o'clock):

$$\varepsilon_{l,1} = \varepsilon_a + \varepsilon_{b,max} \sin\theta, \tag{3.6}$$

$$\varepsilon_{l,2} = \varepsilon_a + \varepsilon_{b,max} \sin\left(\theta + \frac{2\pi}{3}\right), \tag{3.7}$$

$$\varepsilon_{l,3} = \varepsilon_a + \varepsilon_{b,max} \sin\left(\theta + \frac{4\pi}{3}\right). \tag{3.8}$$

After some manipulation,

$$\varepsilon_a = \frac{\varepsilon_{l,1} + \varepsilon_{l,2} + \varepsilon_{l,3}}{3}, \tag{3.9}$$

$$\theta = \tan^{-1}\left[\frac{2\varepsilon_{l,1} - \varepsilon_{l,2} - \varepsilon_{l,3}}{\sqrt{3}(\varepsilon_{l,2} - \varepsilon_{l,3})}\right], \tag{3.10}$$

$$\varepsilon_{b,max} = \frac{\varepsilon_{l,2} - \varepsilon_{l,3}}{\sqrt{3}} \tag{3.11}$$

if $\theta = 0$, π or else

$$\varepsilon_{b,max} = \frac{2\varepsilon_{l,1} - \varepsilon_{l,2} - \varepsilon_{l,3}}{3 \sin\theta}. \tag{3.12}$$

Two such triads of FBG gauges were clamped (the material, chosen by reason of its relatively high α, repels most commercial adhesives) to a 1-m-long polyethylene tube (connected to a supply of hot water and equipped with brass terminal fittings as well as frictionless alignment gates, all bolted or

screwed to a spruce board): the first close to the inlet; the second roughly at the centre of a pre-existing bend, exploited to "catalyse" buckling (v. § 1.2). A p of 1 bar (as read on the dial of the manometers) was attained by partially opening the outlet valve; the average T regularly measured with an infrared thermometer; ε_l acquired by an interrogator, transferred to a computer, saved in a text file (excerpted in Appendix 4) and processed in MATLAB (v. Appendix 5). For details, consult Tables 1.1, 2.1 and Figs. 3.2-4 (made in AutoCAD).

3.2 RESULTS

As evidenced by Fig. 3.6, Triad 1 (sensors 1-3) registered an increment in tensile strain (positive); instead, Triad 2 recorded concurrent expansion in the upper portion (sensor 4) and contraction in the lower one (sensors 5-6). The traces ultimately transform into uninterpretable parallel lines on account of temperature compensation (v. § 2.3).

The bending behaviour is not necessarily indicative of buckling, being observable also in the phases preceding or succeeding this event, which can nonetheless be unequivocally identified by distinctive trends of ε_a and ε_b, extracted from ε_l (v. Fig. 3.1b-c). Fig. 3.7 reveals that the tension encountered in the inceptive stage (attributable to the instantaneous contact with the heating fluid) was gradually counterbalanced by the reaction of the constraint at the outlet, perceived first by Triad 2, undergoing sudden compression and subsequently releasing it (a circumstance compatible with geometric shortening – v. § 1.1). Fig. 3.8 "inserts the missing piece in the jigsaw" by evincing a surge in ε_b within the bend.

3.3 CLOSING REMARKS

To recapitulate,

- *upheaval buckling* is *a mechanism whereby a segment of buried pipeline bows upwards out of the trench under excessive axial compression* (Preface);
- *the possibility that overstress may culminate in rupture strongly calls for the adoption of* successful *monitoring systems* (ibid.);
- *today fibre-optic sensors offer an attractive alternative to their conventional electrical counterpart* (ibid.);
- unfortunately, *the apparent thermal strain can fatally vitiate measurements* (§ 2.3);
- this disadvantage notwithstanding, our experiment verified the potential of FBG gauges to "diagnose" buckling in a correct and prompt manner.

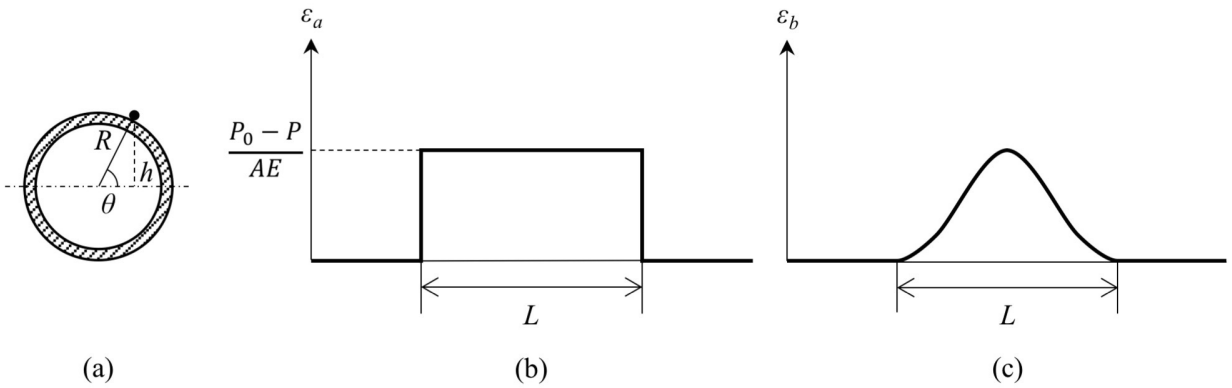

FIG. 3.1 (a) Cross-section of a buckled pipe. Distributions of (b) ε_a and (c) ε_b.

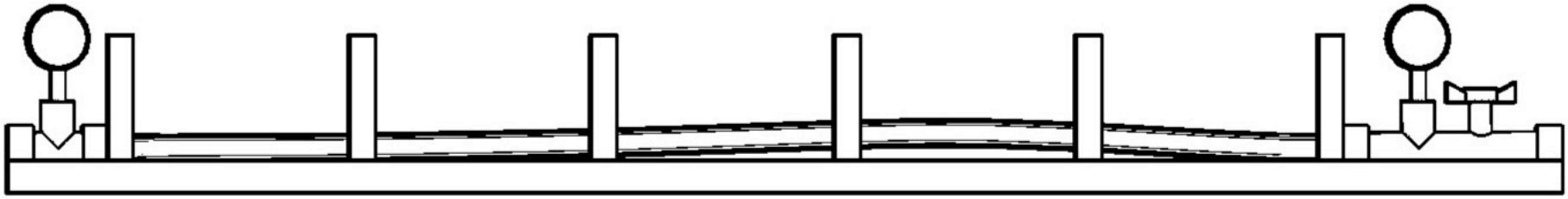

(a)

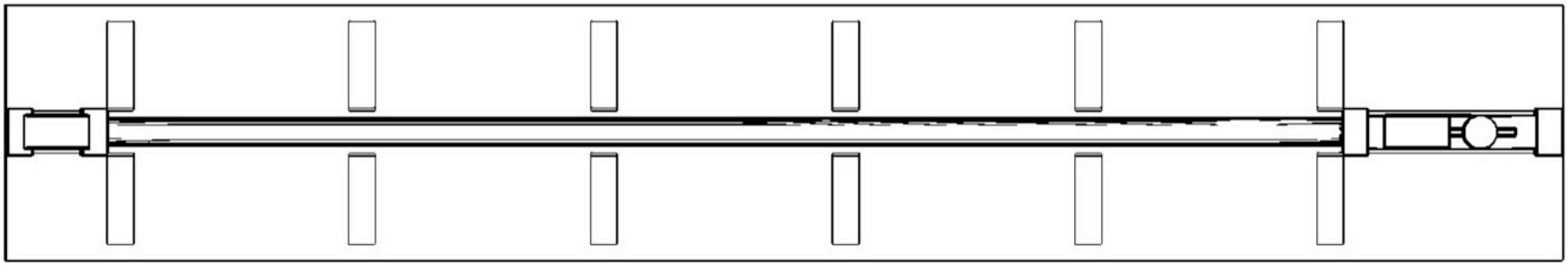

(b)

FIG. 3.2 (a) Front and (b) top views of the apparatus (scale 1:5).

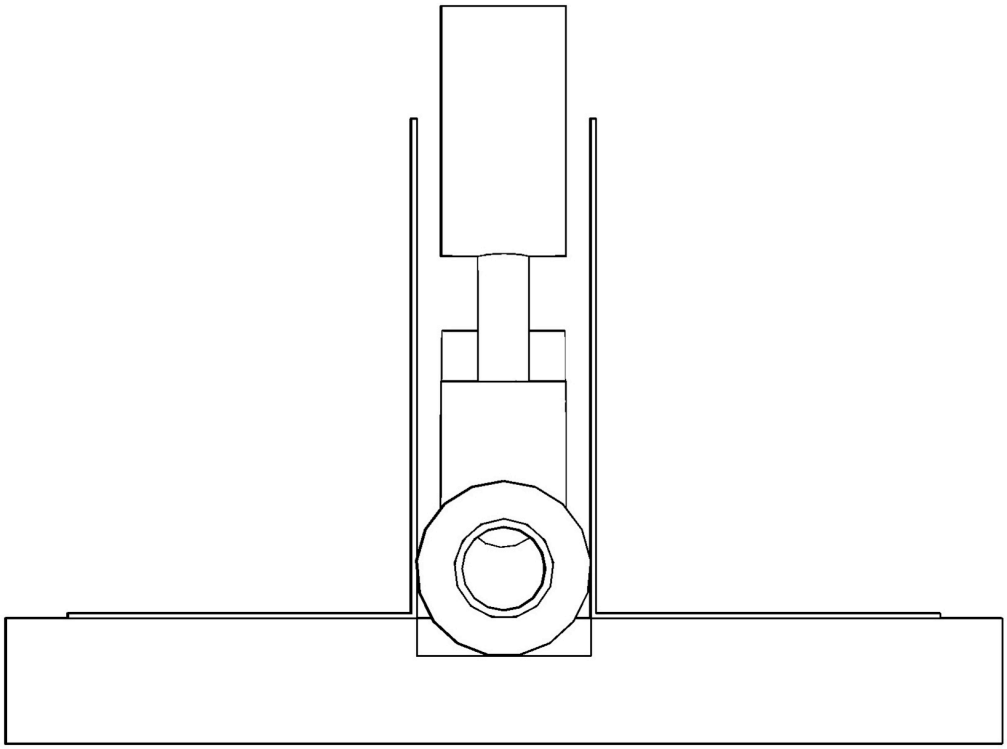

(a)

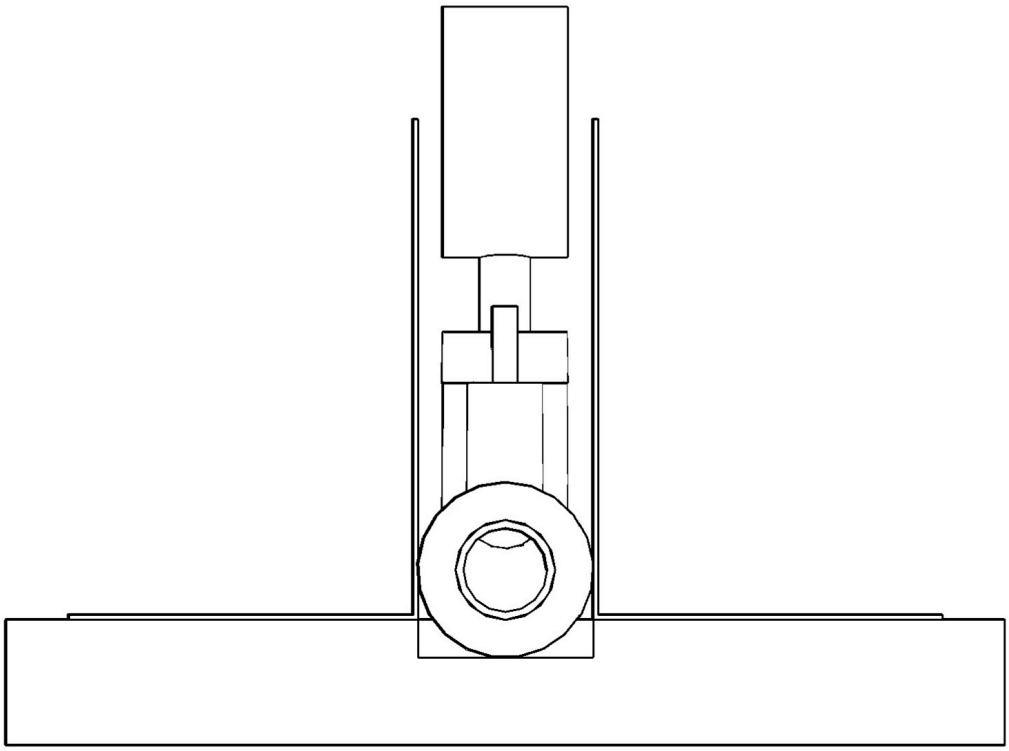

(b)

FIG. 3.3 (a) Left and (b) right views of the apparatus (scale 1:1.5).

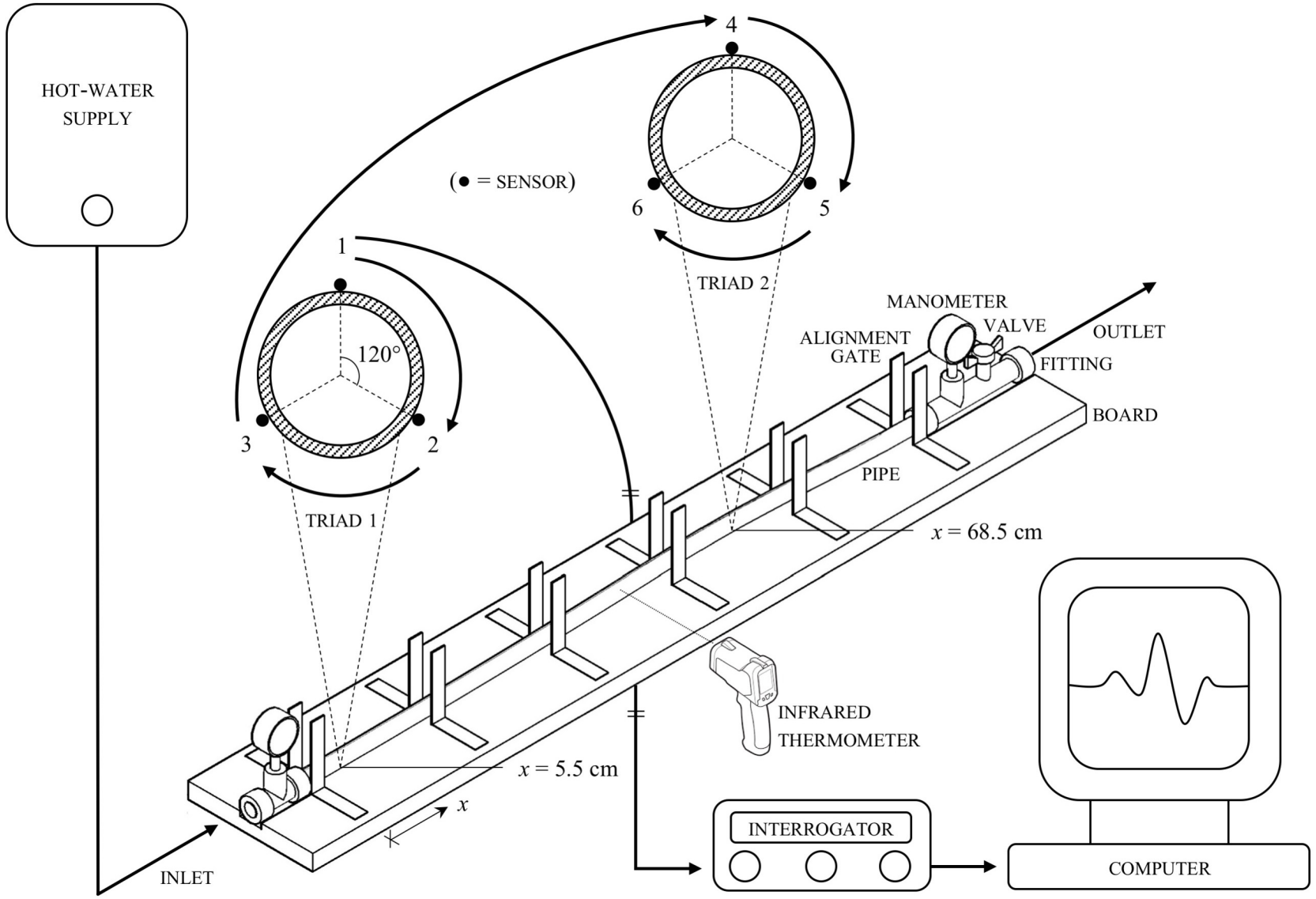

FIG. 3.4 Diagram of the experiment.

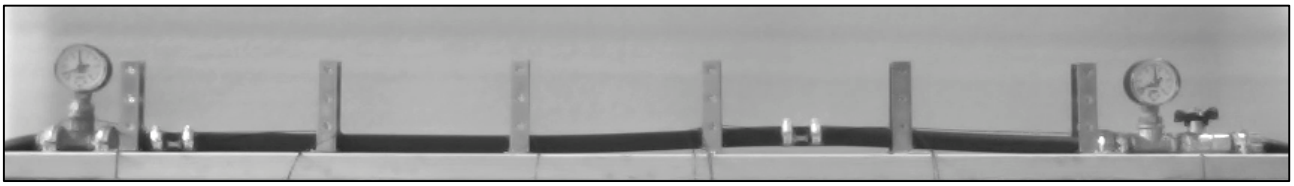

(Time = 0 s)

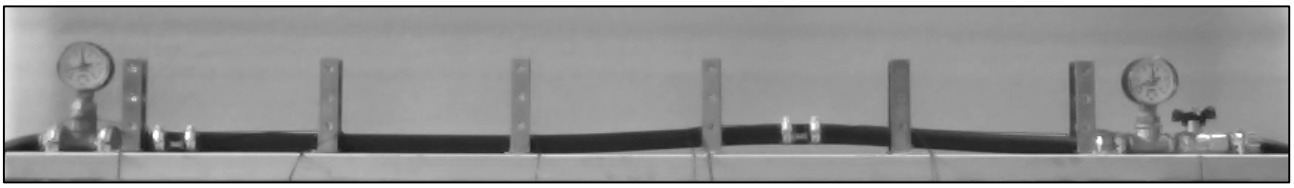

(Time = 5 s)

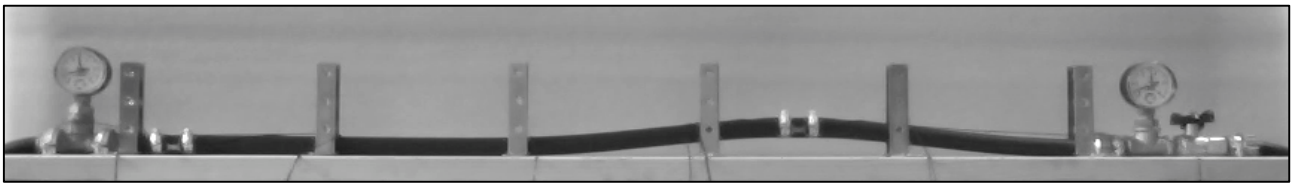

(Time = 10 s)

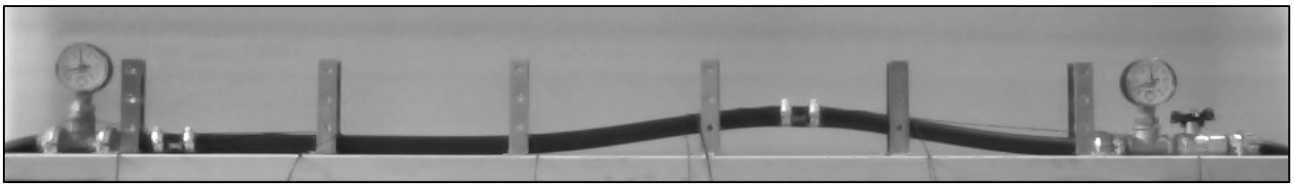

(Time = 15 s)

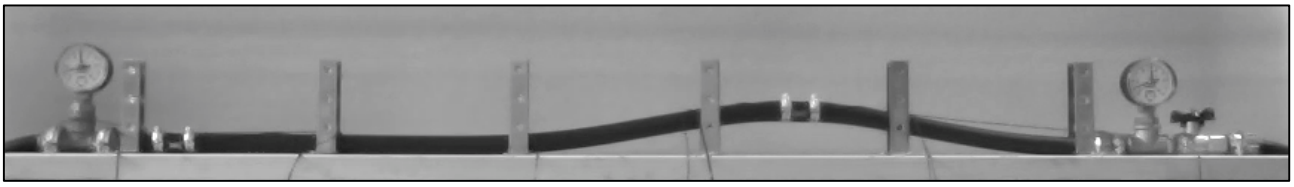

(Time = 20 s)

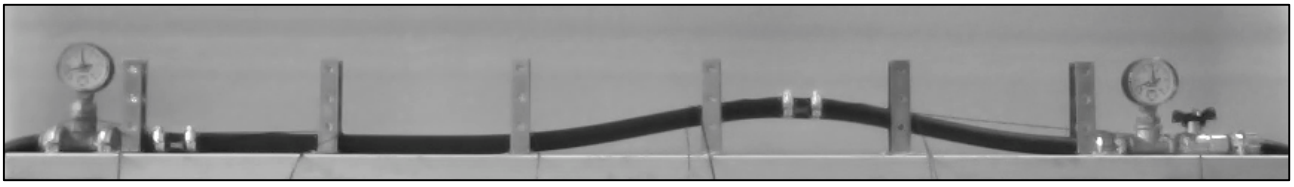

(Time = 25 s)

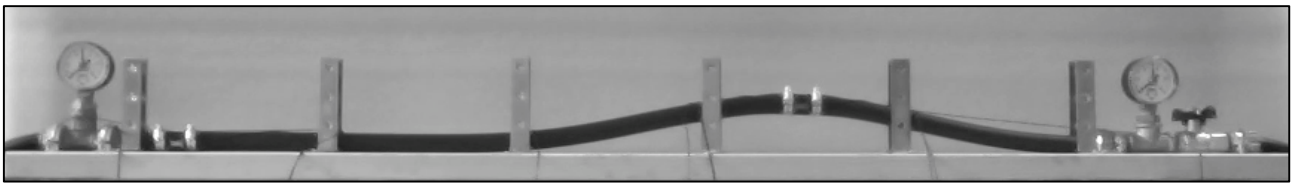

(Time = 30 s)

FIG. 3.5 Selected frames from the video of the experiment.

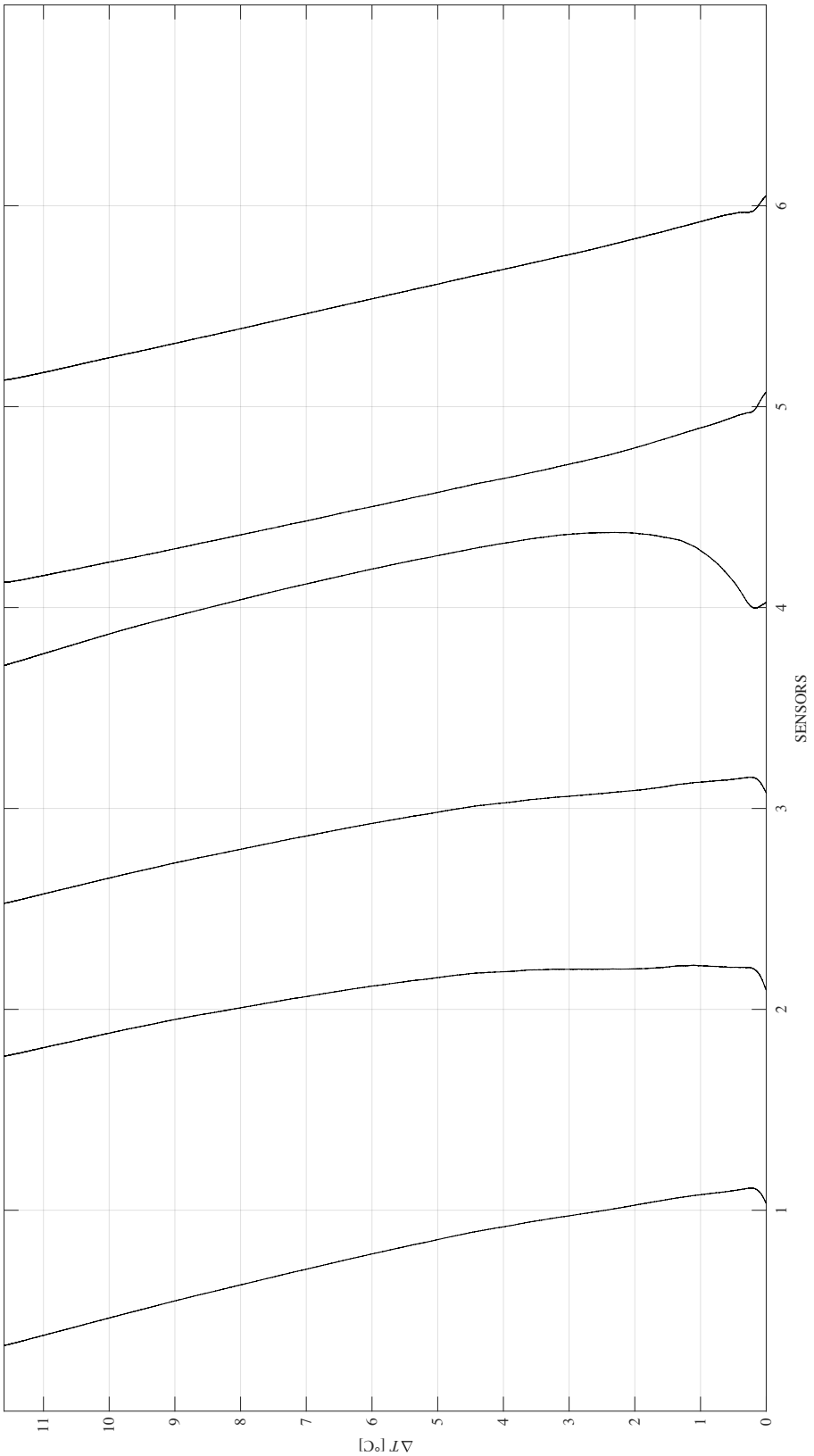

FIG. 3.6 ΔT vs temperature-compensated ε_l for Triads 1 (sensors 1-3) and 2 (sensors 4-6).

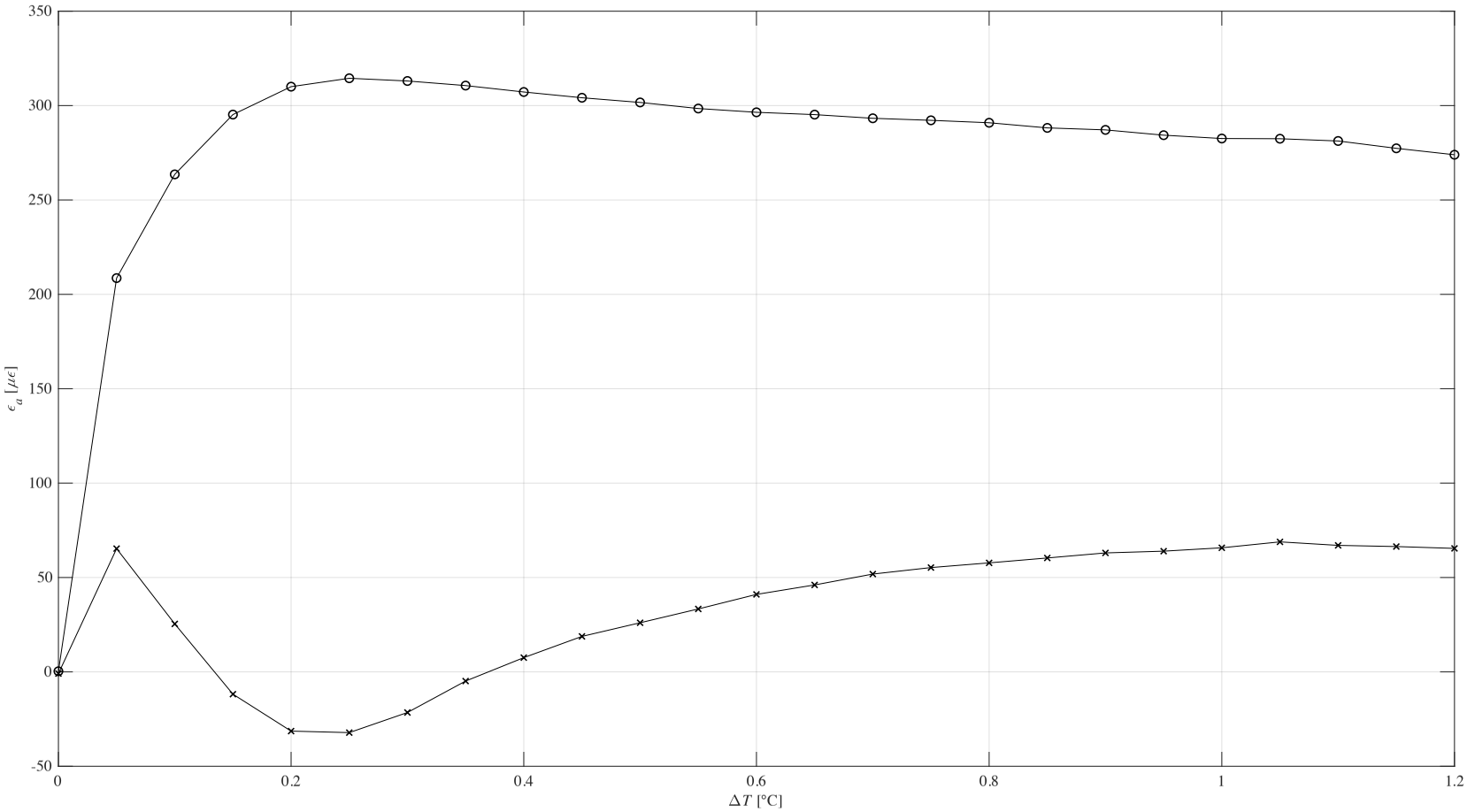

FIG. 3.7 ε_a vs ΔT for Triads 1 (○) and 2 (×).

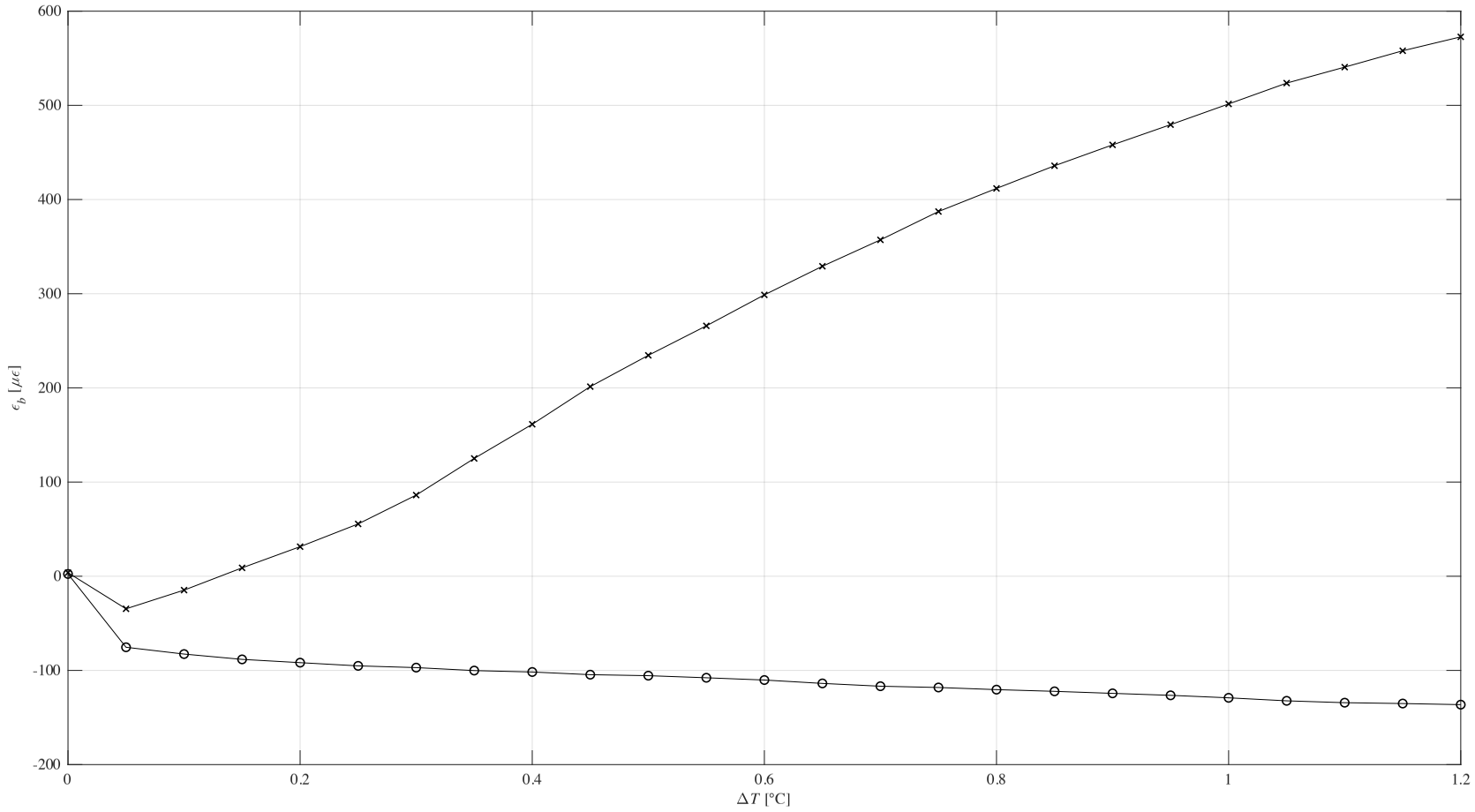

FIG. 3.8 ε_b vs ΔT for Triads 1 (○) and 2 (×).

APPENDIX 1

$EI\frac{d^4y}{dx^4} + P\frac{d^2y}{dx^2} + w = 0 \Rightarrow$ ..... (1.12)
$\Rightarrow EIy'''' + Py'' = -w$ ..... (I)

This is a 4th-order linear inhomogeneous ODE with constant coefficients.

COMPLEMENTARY FUNCTION

$EI\rho^4 + P\rho^2 = 0$

$\rho^2(EI\rho^2 + P) = 0$

$\rho^2 = 0 \Rightarrow$
$\Rightarrow \rho_1 = 0$

$EI\rho^2 + P = 0 \Rightarrow$
$\Rightarrow \rho_{2,3} = \pm i\sqrt{\frac{P}{EI}} =$
$= 0 \pm im =$
$= \tau \pm i\omega$

$y_0(x) = k_1 e^{\rho_1 x} + e^{\tau x}[k_2 \cos(\omega x) + k_3 \sin(\omega x)] =$
$= k_1 + k_2 \cos(mx) + k_3 \sin(mx)$

PARTICULAR INTEGRAL

$y_p(x) = \beta x^2 + \gamma x + \delta$

$y_p' = 2\beta x + \gamma$

$y_p'' = 2\beta$

$y_p''' = 0$

$y_p'''' = 0$

$P2\beta = -w \Rightarrow$
$\Rightarrow \beta = -\frac{w}{2P}$ ..... from (I)

$y_p(x) = -\frac{wx^2}{2P} + \gamma x + \delta$

GENERAL INTEGRAL

$$y(x) = y_0(x) + y_p(x) =$$
$$= k_1 + k_2\cos(mx) + k_3\sin(mx) - \frac{wx^2}{2P} + \gamma x + \delta =$$
$$= k_1^* + k_2\cos(mx) + k_3\sin(mx) - \frac{wx^2}{2P} + \gamma x$$

BOUNDARY CONDITIONS

$$y\left(\frac{L}{2}\right) = k_1^* + k_2\cos\left(\frac{mL}{2}\right) + k_3\sin\left(\frac{mL}{2}\right) - \frac{wL^2}{8P} + \frac{\gamma L}{2} = 0 \quad \text{..... (II), from (1.14)}$$

$$y\left(-\frac{L}{2}\right) = k_1^* + k_2\cos\left(-\frac{mL}{2}\right) + k_3\sin\left(-\frac{mL}{2}\right) - \frac{wL^2}{8P} - \frac{\gamma L}{2} =$$
$$= k_1^* + k_2\cos\left(\frac{mL}{2}\right) - k_3\sin\left(\frac{mL}{2}\right) - \frac{wL^2}{8P} - \frac{\gamma L}{2} = 0 \quad \text{..... (III), from (1.14)}$$

$$y'\left(\frac{L}{2}\right) = -k_2\sin\left(\frac{mL}{2}\right)m + k_3\cos\left(\frac{mL}{2}\right)m - \frac{wL}{2P} + \gamma = 0 \quad \text{..... (IV), from (1.15)}$$

$$y'\left(-\frac{L}{2}\right) = -k_2\sin\left(-\frac{mL}{2}\right)m + k_3\cos\left(-\frac{mL}{2}\right)m + \frac{wL}{2P} + \gamma =$$
$$= k_2\sin\left(\frac{mL}{2}\right)m + k_3\cos\left(\frac{mL}{2}\right)m + \frac{wL}{2P} + \gamma = 0 \quad \text{..... (V), from (1.15)}$$

$$\text{(II)} + \text{(III)} = 2k_1^* + 2k_2\cos\left(\frac{mL}{2}\right) - \frac{wL^2}{4P} = 0 \Rightarrow$$
$$\Rightarrow k_1^* = -k_2\cos\left(\frac{mL}{2}\right) + \frac{wL^2}{8P} \quad \text{..... (VI)}$$

$$\text{(IV)} + \text{(V)} = 2k_3\cos\left(\frac{mL}{2}\right)m + 2\gamma = 0 \Rightarrow$$
$$\Rightarrow \gamma = -k_3\cos\left(\frac{mL}{2}\right)m \quad \text{..... (VII)}$$

$$-k_2\cos\left(\frac{mL}{2}\right) + \frac{wL^2}{8P} + k_2\cos\left(\frac{mL}{2}\right) + k_3\sin\left(\frac{mL}{2}\right) - \frac{wL^2}{8P} - k_3\cos\left(\frac{mL}{2}\right)\frac{mL}{2} =$$
$$= k_3\left[\sin\left(\frac{mL}{2}\right) - \cos\left(\frac{mL}{2}\right)\frac{mL}{2}\right] = 0 \Rightarrow$$
$$\Rightarrow k_3 = 0 \Rightarrow \quad \text{..... from (II)}$$
$$\Rightarrow \gamma = 0 \quad \text{..... from (VII)}$$

$$k_2 = -\left(k_1^* - \frac{wL^2}{8P}\right)\frac{1}{\cos(mL/2)} \quad \text{..... (VIII), from (VI)}$$

$$\left(k_1^* - \frac{wL^2}{8P}\right)\frac{\sin(mL/2)}{\cos(mL/2)}m - \frac{wL}{2P} =$$
$$= \left(k_1^* - \frac{wL^2}{8P}\right)\tan\left(\frac{mL}{2}\right)m - \frac{wL}{2P} =$$
$$= \left(k_1^* - \frac{wL^2}{8P}\right)\frac{m^2L}{2} - \frac{wL}{2P} = 0 \Rightarrow$$
$$\Rightarrow k_1^* = \frac{wL^2}{8P} + \frac{w}{m^2P} \Rightarrow \quad \text{..... from (IV)}$$

$$\Rightarrow k_2 = -\frac{w}{m^2 P \cos(mL/2)} \quad \text{..... from (VIII)}$$

SOLUTION

$$y(x) = \frac{wL^2}{8P} + \frac{w}{m^2 P} - \frac{w\cos(mx)}{m^2 P \cos(mL/2)} - \frac{wx^2}{2P} =$$

$$= \frac{wEI}{P^2}\left[1 + \frac{m^2 L^2}{8} - \frac{m^2 x^2}{2} - \frac{\cos(mx)}{\cos(mL/2)}\right] \quad \text{..... (1.17)}$$

APPENDIX 2

```
clear all
close all
```

```
%% INPUT (from Table 1.1)
D = 20; %[mm]
t = 1.6; %[mm]
w = 0.000934; %[N/mm]
E = 200; %[N/mm^2]
```

```
%% CALCULATIONS
d = D-2*t;
A = (pi/4)*(D^2-d^2);
I = (pi/64)*(D^4-d^4);
Lmin = (1.69*10^6*((E*I)^3/(w^2*A*E)))^0.125; %(1.26)
L = 0.1*Lmin:1:3*Lmin;
P = 80.8*((E*I)./L.^2); %(1.21)
P0 = P+16.0*10^-6*((w^2*A*E.*L.^6)/(E*I)^2); %(1.25)
Lmaxslope = (11.6*((E*I)/w))^0.333; %From eq. 12 in Ref. 8
```

```
%% OUTPUT
fig = figure(); %Fig. 1.4
plot(L./10^3,P0,'-k',L./10^3,P,'--k');
xlim([0 5]);
ylim([0 100]);
line([Lmaxslope/10^3 Lmaxslope/10^3],[0 100],'Color','k','LineStyle','-.');
xlabel('{\itL} [m]');
ylabel('{\itP}_0, {\itP} [N]');
txt = text(Lmaxslope/10^3,25,'\leftarrow Max. slope = 0.1');
set(findall(fig,'-property','FontName'),'FontName','Times New Roman','FontSize',11);
grid on;
```

APPENDIX 3

```
clear all

close all
```

```
%% DATA

p = 80; %[bar] (*)

D = 48; %[in.] (*)

t = 0.462; %[in.] (*)

wpipe = 235; %[lbf/ft] (**)

SWoil = 300.5; %[lbf/bbl] (**)

SWfill = 1500; %[kgf/m^3] (***)

hfill = 8; %[ft] (**)

E = 200; %[GPa] (****)

aH = 12*10^-6; %[/°C] (****)

nu = 0.3; %(****)

aF = 0.7; %[microstrain/°C] %(*****)

Se = 10^-6; %[/microstrain] %(*****)

ST = 6.156*10^-6; %[/°C] %(*****)

%(*) Table 1 / (**) 2013 TAPS Fact Book / Typical values for (***) gravel, (****) steel / (*****) Table 2.1
```

```
%% CONVERSIONS

p = p*10^5; %[Pa]

D = D*0.0254; %[m]

t = t*0.0254; %[m]

wpipe = wpipe*1.35582; %[N/m]

SWoil = SWoil*2.85; %[kgf/m^3]

hfill = hfill*0.3048; %[m]

E = E*10^9; %[Pa]
```

```
%% CALCULATIONS

d = D-2*t;

A = (pi/4)*(D^2-d^2);

I = (pi/64)*(D^4-d^4);

woil = SWoil*((pi/4)*d^2);

wfill = SWfill*hfill*D;

w = wpipe+woil+wfill;

Lmin = (1.69*10^6*((E*I)^3/(w^2*A*E)))^0.125; %(1.26)

P = 80.8*((E*I)/Lmin^2); %(1.21)

P0 = P+16.0*10^-6*((w^2*A*E*Lmin^6)/(E*I)^2); %(1.25)

dT = (1/(A*E*aH))*(P0-(((0.5-nu)*A*p*(D/2))/t)) %(1.5)

strain = ((P0-P)/(A*E))*10^6 %(1.24), (3.3)

tempcomp = ((aH/10^-6)-aF+(ST/Se))*dT %(2.17)
```

APPENDIX 4

TIME	SENSOR_1	SENSOR_2	SENSOR_3	SENSOR_4	SENSOR_5	SENSOR_6
07/06/2019 16:09:29.667	2.737	-1.124	-0.625	2.884	-1.762	-3.784
07/06/2019 16:09:29.668	3.857	-0.500	0.624	2.007	-1.762	-2.397
07/06/2019 16:09:29.669	3.235	-1.124	-0.251	3.386	-1.636	-4.792
07/06/2019 16:09:29.670	3.733	0.624	0.125	4.514	-1.133	-3.531
07/06/2019 16:09:29.671	3.359	-0.873	-0.251	3.134	-1.384	-4.792
07/06/2019 16:09:29.672	3.982	-0.873	0.000	3.261	-1.888	-2.648
07/06/2019 16:09:29.673	2.365	0.000	0.875	2.884	-2.013	-3.909
07/06/2019 16:09:29.674	3.857	-1.748	0.624	3.134	-0.882	-4.792
07/06/2019 16:09:29.675	3.733	-0.873	-0.625	3.386	-1.888	-4.287
07/06/2019 16:09:29.676	2.861	0.000	0.000	2.884	-3.146	-3.909
07/06/2019 16:09:29.677	2.489	-0.624	0.375	2.884	-2.139	-4.035
07/06/2019 16:09:29.678	2.861	-0.873	0.375	3.511	-2.139	-4.161
07/06/2019 16:09:29.679	3.111	-0.873	-0.625	3.762	-1.007	-2.900
07/06/2019 16:09:29.680	3.111	-0.500	0.250	3.887	-1.636	-5.171
07/06/2019 16:09:29.681	3.484	-0.500	1.000	3.636	-2.895	-3.784
07/06/2019 16:09:29.682	3.608	-1.124	-0.376	3.009	-0.882	-3.026
07/06/2019 16:09:29.683	3.733	-1.248	0.875	2.507	-1.888	-3.909
07/06/2019 16:09:29.684	3.111	-0.624	-0.876	2.382	-2.391	-3.909
07/06/2019 16:09:29.685	2.613	-1.124	0.125	3.386	-2.139	-3.909
07/06/2019 16:09:29.686	3.733	-1.124	-0.501	2.759	-1.636	-4.035
07/06/2019 16:09:29.687	3.359	-0.873	0.000	3.009	-1.636	-3.531
07/06/2019 16:09:29.688	2.489	-0.624	0.875	2.884	-2.139	-4.792
07/06/2019 16:09:29.689	2.489	-1.748	-0.251	3.386	-1.384	-3.784
07/06/2019 16:09:29.690	3.111	-1.124	0.250	3.261	-1.384	-4.161
07/06/2019 16:09:29.691	2.986	-0.873	0.624	2.382	-2.517	-3.784
07/06/2019 16:09:29.692	3.982	-1.124	0.375	2.884	-1.888	-3.153
07/06/2019 16:09:29.693	2.986	-1.498	0.125	2.507	-2.139	-4.161
07/06/2019 16:09:29.694	3.484	-1.124	-1.502	4.013	-1.384	-3.909
07/06/2019 16:09:29.695	3.608	0.375	-1.126	2.507	-2.139	-4.792
07/06/2019 16:09:29.696	2.861	-0.873	-0.126	3.134	-1.007	-3.531
07/06/2019 16:09:29.697	2.613	-1.124	-0.625	3.134	-2.895	-5.171
07/06/2019 16:09:29.698	3.608	-1.124	0.750	2.634	-1.636	-2.900
07/06/2019 16:09:29.699	2.986	-0.873	0.250	2.759	-1.636	-3.279
07/06/2019 16:09:29.700	2.861	-0.624	0.624	3.261	-2.266	-4.161
07/06/2019 16:09:29.701	2.613	-0.624	-0.876	3.134	-1.133	-4.918
07/06/2019 16:09:29.702	2.737	0.125	-0.376	2.257	-2.517	-4.161
07/06/2019 16:09:29.703	1.867	-0.624	-0.501	2.759	-1.762	-3.909
07/06/2019 16:09:29.704	2.861	-1.124	-0.251	3.009	-1.384	-4.792
07/06/2019 16:09:29.705	2.861	-1.498	0.375	3.009	-1.762	-4.161
07/06/2019 16:09:29.706	3.733	-1.622	0.000	3.009	-1.258	-2.018
07/06/2019 16:09:29.707	2.613	-1.748	-0.126	2.507	-2.642	-2.648
07/06/2019 16:09:29.708	2.613	-1.124	-0.501	3.261	-2.517	-4.792
07/06/2019 16:09:29.709	2.613	-1.748	0.375	4.138	-2.391	-4.161
07/06/2019 16:09:29.710	3.359	-1.124	-0.126	1.880	-1.258	-4.413
07/06/2019 16:09:29.711	3.111	-1.124	0.499	3.009	-2.139	-3.784
07/06/2019 16:09:29.712	2.861	-1.748	-0.501	3.887	-1.762	-4.161
07/06/2019 16:09:29.713	3.608	0.000	-0.501	3.134	-1.636	-3.909
07/06/2019 16:09:29.714	2.365	0.125	0.000	2.382	-2.642	-3.656
07/06/2019 16:09:29.715	2.365	-1.748	-0.625	3.511	-1.636	-3.909
07/06/2019 16:09:29.716	3.484	-0.500	0.125	3.134	-1.007	-3.656
07/06/2019 16:09:29.717	4.106	-0.873	-0.251	3.636	-2.266	-2.900
07/06/2019 16:09:29.718	2.489	-0.873	0.624	3.636	-1.384	-3.531
07/06/2019 16:09:29.719	3.235	0.375	-0.376	2.884	-2.642	-3.026
07/06/2019 16:09:29.720	2.861	-1.498	-0.501	3.762	-1.762	-5.171
07/06/2019 16:09:29.721	2.489	-0.624	-0.501	2.759	-0.755	-3.784
07/06/2019 16:09:29.722	3.608	-0.873	0.375	3.511	-1.762	-4.792
07/06/2019 16:09:29.723	2.986	-0.500	0.375	2.884	-0.882	-3.026
07/06/2019 16:09:29.724	2.365	-1.248	-0.126	3.134	-1.888	-3.279
07/06/2019 16:09:29.725	2.986	-0.249	0.375	3.386	-1.762	-3.909
07/06/2019 16:09:29.726	3.235	-0.873	-0.251	2.507	-1.762	-3.531
07/06/2019 16:09:29.727	2.861	-1.498	0.375	3.386	-1.888	-3.531
07/06/2019 16:09:29.728	3.733	-1.124	-0.376	2.507	-1.762	-3.784
07/06/2019 16:09:29.729	2.489	-0.249	-0.625	2.759	-2.642	-2.018
07/06/2019 16:09:29.730	2.986	-0.249	1.000	4.138	-1.384	-3.026
07/06/2019 16:09:29.731	2.861	-1.248	0.624	2.884	-1.762	-4.540
07/06/2019 16:09:29.732	3.359	-0.624	0.624	3.511	-1.258	-4.161
07/06/2019 16:09:29.733	3.235	0.125	0.375	3.134	-1.133	-2.522
07/06/2019 16:09:29.734	3.733	-0.500	-0.501	3.386	-2.391	-3.531
07/06/2019 16:09:29.735	3.359	-0.500	-0.126	2.634	-1.636	-3.279
07/06/2019 16:09:29.736	3.111	-1.124	0.750	3.762	-1.133	-3.909
07/06/2019 16:09:29.737	3.111	0.749	-0.501	4.013	-1.384	-3.909
07/06/2019 16:09:29.738	2.861	-0.624	0.875	2.759	-1.384	-3.279
07/06/2019 16:09:29.739	4.355	-0.624	0.499	3.134	-1.007	-4.540
07/06/2019 16:09:29.740	2.861	-0.249	0.875	3.386	-2.013	-3.909
07/06/2019 16:09:29.741	3.733	-0.249	0.000	3.134	-1.133	-2.522
07/06/2019 16:09:29.742	3.111	0.000	2.376	2.884	-0.882	-4.035
07/06/2019 16:09:29.743	3.982	0.375	1.625	3.386	-1.258	-4.918
07/06/2019 16:09:29.744	4.355	0.000	0.499	3.386	-0.882	-4.792

[...]

APPENDIX 5

```
function FBG_Strain_Gauge_Data_Analysis_Tool()
```

```
clear all

close all
```

```
%% INPUT

aH = 200; %[microstrain/°C] (*)

aF = 0.7; %[microstrain/°C] (**)

Se = 10^-6; %[/microstrain] (**)

ST = 6.156*10^-6; %[/°C] (**)

time1 = 10; %[s]

time2 = 20; %[s]

time3 = 30; %[s]

T0 = 23.8; %[°C] (***)

T1 = 25.6; %[°C] (***)

T2 = 31.4; %[°C] (***)

T3 = 35.4; %[°C] (***)

%(*) Table 1.1 / (**) Table 2.1 / (***) Measured
```

```
%% IMPORT DATA FROM TEXT FILE

[filename,~] = uigetfile({'*.txt'},'Please, choose a file:');

delimiter = '\t';

if nargin <= 2

   startRow = 2;

   endRow = inf;

end

formatSpec = '%*q%f%f%f%f%f%[^\n\r]';

fileID = fopen(filename,'r');

textscan(fileID,'%[^\n\r]',startRow-1,'WhiteSpace','','ReturnOnError',false);

dataArray = textscan(fileID,formatSpec,endRow-startRow+1,'Delimiter',delimiter,'TextType','string',...
            ...'EmptyValue',NaN,'ReturnOnError',false,'EndOfLine','\r\n');

fclose(fileID);

strain = [dataArray{1:end-1}];

clearvars filename delimiter startRow endRow formatSpec fileID dataArray ans;

[a,~] = size(strain);

time = [0,time1,time2,time3];

T_meas = [T0,T1,T2,T3];

regr = polyfit(time,T_meas,3);

for i = 1:6

    for ii = 1:1:a

        T_int(ii,i) = regr(1)*((ii-1)*10^-3)^3+regr(2)*((ii-1)*10^-3)^2+regr(3)*((ii-1)*10^-3)+T0;

    end

end
```

```
dT = T_int-T0;
strain_c = strain-((aH-aF+ST/Se).*dT); %(2.16-17)
```

```
%% CALCULATIONS AND OUTPUT
fig1 = figure(); %Fig. 3.6
dT_T = transpose(dT(:,1));
x = (1:6);
wiggle(x,dT_T,strain_c,'wiggle',2000);
axis([0 max(x)+1 0 max(dT_T)]);
xticks(1:max(x));
yticks(0:max(dT_T));
xlabel('SENSORS');
ylabel('\Delta{\itT} [°C]');
grid on;
%(3.9-12):
iii = 1;
for iv = 0:0.05:1.2
    k = find(dT_T >= iv,1);
    ea1(iii) = (strain_c(k,1)+strain_c(k,2)+strain_c(k,3))/3;
    theta1 = atan((2*strain_c(k,1)-strain_c(k,2)-strain_c(k,3))/(sqrt(3)*(strain_c(k,2)-strain_c(k,3))));
    if (theta1 == 0) || (theta1 == pi)
       eb1_max = (strain_c(k,2)-strain_c(k,3))/sqrt(3);
    else
       eb1_max = (2*strain_c(k,1)-strain_c(k,2)-strain_c(k,3))/(3*sin(theta1));
    end
    eb1(iii) = eb1_max*sin(theta1);
    ea2(iii) = (strain_c(k,4)+strain_c(k,5)+strain_c(k,6))/3;
    theta2 = atan((2*strain_c(k,4)-strain_c(k,5)-strain_c(k,6))/(sqrt(3)*(strain_c(k,5)-strain_c(k,6))));
    if (theta2 == 0) || (theta2 == pi)
       eb2_max = (strain_c(k,5)-strain_c(k,6))/sqrt(3);
    else
       eb2_max = (2*strain_c(k,4)-strain_c(k,5)-strain_c(k,6))/(3*sin(theta2));
    end
    eb2(iii) = eb2_max*sin(theta2);
    iii = iii+1;
end
fig2 = figure(); %Fig. 3.7
plot(0:0.05:1.2,ea1,'-ok',0:0.05:1.2,ea2,'-xk');
xlabel('\Delta{\itT} [°C]');
ylabel('{\it\epsilon}_{{\ita}} [{\it\mu\epsilon}]');
grid on;
fig3 = figure(); %Fig. 3.8
plot(0:0.05:1.2,eb1,'-ok',0:0.05:1.2,eb2,'-xk');
xlabel('\Delta{\itT} [°C]');
```

```
ylabel('{\it\epsilon}_{{\itb}} [{\it\mu\epsilon}]');
grid on;
set(findall(fig1,'-property','FontName'),'FontName','Times New Roman','FontSize',11);
set(findall(fig2,'-property','FontName'),'FontName','Times New Roman','FontSize',11);
set(findall(fig3,'-property','FontName'),'FontName','Times New Roman','FontSize',11);
```

```
function wiggle(x,t,Data,style,dmax,showmax,plImage,imageax,~) %(C) 2004 Thomas Mejer Hansen
```

```
if (nargin == 9)
   np=3;
   subplot(np,np,1);
   wiggle(Data);
   subplot(np,np,2);
   wiggle(Data,dmax);
   subplot(np,np,3);
   wiggle(x,t,Data);
   subplot(np,np,4);
   wiggle(x,t,Data,style,dmax);
   subplot(np,np,5);
   wiggle(x,t,Data,style,dmax,showmax);
   subplot(np,np,6);
   wiggle(x,t,Data,style,dmax,showmax,plImage);
      if isempty(dmax)
         dmax = nanmax(abs(Data(:)));
      end
   subplot(np,np,7);
   wiggle(x,t,Data,style,dmax,showmax,plImage,dmax./10);
   return
end
showmax_def = 100;
style_def = 'wiggle';
if (nargin == 1)
   Data = x;
   t = [1:1:size(Data,1)];
   x = [1:1:size(Data,2)];
   dmax = max(Data(:));
   style = style_def;
   showmax = showmax_def;
end
if (nargin == 2)
   Data = x;
   dmax = t;
   t = [1:1:size(Data,1)];
```

```
   x = [1:1:size(Data,2)];
   style = style_def;
   showmax = showmax_def;
end
if (nargin == 3)
   style = style_def;
   dmax = nanmax(abs(Data(:)));
   showmax = showmax_def;
end
if (nargin == 4)
   dmax = nanmax(abs(Data(:)));
   showmax = showmax_def;
end
if (nargin == 5)
   showmax = showmax_def;
end
if (nargin < 7)
   plImage =0;
end
if isempty(dmax)
   dmax = nanmax(abs(Data(:)));
end
if isempty(showmax)
   showmax=100;
end
if (nargin == 7)
   imageax = [-1 1].*dmax;
end
if (plImage == 1)
   imagesc(x,t,Data);
   if (length(imageax) == 1)
      imageax = [-1 1].*abs(imageax);
   end
   caxis(imageax);
   hold on;
end
if (showmax > 0)
   if (length(x) > 1)
      dx=x(2)-x(1);
   end
   ntraces = length(x);
   d = ntraces/showmax;
   if (d <= 1);
```

```
      d = 1;
   end
   d = round(d);
   dmax = dmax/d;
   for i=1:d:length(x)
       xt = dx*Data(:,i)'./dmax;
       plot(xt+x(i),t,'k-');
       if (i == 1)
          hold on;
       end
   end
axis([x(1) x(i)+1 min(t) max(t)])
end
hold off;
```

NOMENCLATURE

ENGLISH

A	pipe cross-sectional area
C	buckle contour
D	pipe outer diameter
E	pipe Young's modulus
E_F	optical-fibre Young's modulus
G	reflected spectrum
H	buckle maximum height
h	vertical distance from pipe neutral axis
I	pipe cross-section second moment of area
L	buckle length
M	buckle bending moment
m	$= \sqrt{P/EI}$, wavenumber
n	optical-fibre refractive index
P	buckle normal (axial) force
P_0	pre-buckle normal (axial) force
P_1	P_0 temperature component
P_2	P_0 pressure component
p	pipe internal pressure
Q	interrogation-system ratio
R	pipe outer radius
r	pipe inner radius
S	buckle shear force
S_T	optical-fibre temperature sensitivity
S_ε	optical-fibre strain sensitivity
T	temperature
t	pipe wall thickness
VST	pipe Vicat softening temperature
w	pipe weight per unit length
x	horizontal coordinate (// pipe axis)
y	vertical coordinate ($\perp$ pipe axis)

GREEK

α	coefficient of linear thermal expansion (CLTE)
α_F	optical-fibre CLTE
α_H	host-structure (pipe) CLTE
ε	strain
ε_1	P_1-related strain
ε_2	P_2-related strain
ε_a	ε_l axial component
ε_b	ε_l bending component
ε_l	buckled-pipe longitudinal strain
ε_m	optical-fibre mechanical strain
ε_T	optical-fibre apparent thermal strain
ζ_L	optical-fibre path length
θ	angle with respect to pipe neutral axis
Λ	optical-fibre grating period
Λ_{mask}	phase-mask grating period
λ	optical-fibre wavelength
λ_B	optical-fibre Bragg wavelength
ν	pipe Poisson's ratio
σ	stress
σ_y	pipe yield strength

UNIT CONVERSIONS

bar	×	1.0*	E–01	=	N/mm^2
(	×	1.0*	E+05	=	N/m^2 or Pa)
stb	×	1.589873	E–01	=	sm^3**
in.	×	2.54*	E+01	=	mm
(	×	2.54*	E–02	=	m)
scf	×	2.831685	E–02	=	sm^3**
$\mu\varepsilon$	×	1.0*	E+00	=	μm/m

* Exact factor.

** At the stock-tank (for oil) or standard (for gas) conditions of 15 °C and 101325 Pa (atmospheric pressure).

BIBLIOGRAPHY

1. ANSARI, FARHAD; FENG, XIN; MENG, DEWEI; WU, WENJING; ZHOU, JING – *Distributed monitoring method for upheaval buckling in subsea pipelines with BOTDA sensors*, in *Advances in structural engineering*, SAGE, 2017, vol. 20, no. 2, pp. 180-190.

2. ARREGUI, FRANCISCO; CLAUS, RICHARD O.; MATIAS, IGNACIO – *Optical-fibre sensors*, in *Handbook of optics*, McGraw-Hill, 2001, vol. 4, ch. 15.

3. BROWN, TOM G. – *Optical fibres and fibre-optic communications*, in *Handbook of optics*, op. cit., ch. 1.

4. CALLADINE, CHRISTOPHER R.; MALTBY, TIMOTHY C. – *An investigation into upheaval buckling of buried pipelines (I). Experimental apparatus and some observations*, in *International journal of mechanical sciences*, Elsevier, 1995, vol. 37, no. 9, pp. 943-963.

5. ID. – *An investigation into upheaval buckling of buried pipelines (II). Theory and analysis of experimental observations*, in *International journal of mechanical sciences*, op. cit., pp. 965-983.

6. FARRELL, GERALD; SEMENOVA, YULIYA; SUN, AN; WANG, PENGFEI; WU, QIANG – *High-resolution temperature-insensitive interrogation technique for FBG sensors*, in *Optics and laser technology*, Elsevier, 2009, vol. 42, no. 4, pp. 653-656.

7. HILL, KENNETH O. – *FBGs*, in *Handbook of optics*, op. cit., ch. 9.

8. HOBBS, ROGER E. – *Pipeline buckling caused by axial loads*, in *Journal of constructional-steel research*, Elsevier, 1981, vol. 1, no. 2, pp. 2-10 (republished as *In-service buckling of heated pipelines*, in *Journal of transportation engineering*, ASCE, 1984, vol. 110, no. 2, pp. 175-189).

9. KING, ROGER A.; PALMER, ANDREW C. – *Subsea pipeline engineering*, PennWell, 2008, ch. 14.

10. KLECKERS, THOMAS – *Fibre Bragg sensors compared with electrical strain gauges for use in force measurement. Prospects and potentials*, in *Proceedings of the 19th IMEKO world congress on fundamental and applied metrology (Lisbon, 6-11 September 2009)*, pp. 226-229.

11. MEASURES, RAYMOND M. – *Structural monitoring with fibre-optic technology*, Academic Press, 2001, chs. 5-7.